Biologically Inspired Synthetic Gecko Adhesive from Stiff Polymer Microfiber Arrays

by

Jongho Lee

B.S. (Hanyang University, Seoul) 1998
M.S. (Korea Advanced Institute of Science and Technology, Taejeon) 2003
M.S. (University of California, Berkeley) 2006

A dissertation submitted in partial satisfaction of the
requirements for the degree of
Doctor of Philosophy

in

Mechanical Engineering

in the

GRADUATE DIVISION
of the
UNIVERSITY OF CALIFORNIA, BERKELEY

Committee in charge:
Professor Ronald S. Fearing, Co-Chair
Professor Kyriakos Komvopoulos, Co-Chair
Professor Albert P. Pisano
Professor Robert J. Full

Fall 2008

The dissertation of Jongho Lee is approved:

Co-Chair Date

Co-Chair Date

Date

Date

University of California, Berkeley

Fall 2008

Biologically Inspired Synthetic Gecko Adhesive from Stiff Polymer Microfiber Arrays

by

Jongho Lee

Abstract

Biologically Inspired Synthetic Gecko Adhesive from Stiff Polymer Microfiber Arrays

by

Jongho Lee

Doctor of Philosophy in Mechanical Engineering

University of California, Berkeley

Professor Ronald S. Fearing, Co-Chair

Professor Kyriakos Komvopoulos, Co-Chair

Inspiration from nature and development of nano-micro technology suggest new types of smart adhesive. Gecko's fast wall-climbing and upside-down-walking even on not super clean surfaces provide existence of easily attachable and easily releasable, durable, self-cleaning synthetic adhesive. Developing but limited nano-micro technology makes it possible to see and analyze Gecko's nano-micro structures. However, it is a still challenge to make the same sophisticated structures of Gecko. This work explores achieving the key properties of the natural gecko adhesive with relatively simple nano-micro structures from synthetic materials. Stiff material, comparable to the natural gecko adhesives, was used and surface geometry was modified to achieve the novel adhesion properties. Important properties of the fabricated microfiber ar-

rays were characterized and compared with the natural gecko adhesives with custom made sensor apparatuses. The high-aspect-ratio microfiber arrays showed similar novel properties, including easy attach, easy release, durability, self-cleaning, and directionality, of the natural gecko adhesive.

Professor Ronald S. Fearing
Dissertation Committee Co-Chair

Professor Kyriakos Komvopoulos
Dissertation Committee Co-Chair

To my parents, wife, and kids.

Contents

List of Figures

List of Tables

Acknowledgments

First of all, I would like to thank my family, my wife Yehjie Kim, daughter Lauren S. Lee and another expected child for their love and trust. I also would like to thank my parents, Jaeduck Lee and Seungjae Lee for their endless encouragement and support.

I wish to thank my research adviser, Professor Ronald S. Fearing for giving me a chance to work on this excellent project, endless ideas, and comments. I also want to thank my co-adviser, Professor Kyriakos Komvopoulos and my dissertation committee, Professor Albert P. Pisano and Professor Robert J. Full for their comments and guidance. I am also thankful to my former research adviser Professor Shankar S. Sastry for his generous support.

I am grateful to my colleagues in Biomimetic Milli System lab, Carmel Majidi, Erik Steltz, Stan Baek, Aaron Hoover, Bryan Schubert, Fernando Garcia Bermudez, Paul Birkmeyer, Kevin Peterson, Jason Keller, Kevin Ma and Jeff Hsu for their help, comment and discussion. I also would like thank my collaborators, Professor Kellar Autumn, Nick Gravish, Matt Wilkinson, Professor Roya Maboudian, Brian Bush, Victor Chan, Professor Ali Javey and Hyunhyub Ko.

Chapter 1

Introduction

1.1 Natural Gecko Adhesive

Geckos can climb up and walk upside down on most of surfaces including smooth glass and rough trees. Geckos have attracted many scientists to study how they achieve the unique repetitive adhesion. Early 1900s, Schmidt [54] and Dellit [19] detailed anatomy and physiology of Geckos. In 1965, with help of light and electron microscopes, Ruibal and Ernst [51] identified detailed structures of different species of geckos. The anoline setae were simple structures usually less than 30 μm in length and with a single terminal spatula. In contrast, the setae of geckos were complex structures of about 100 μm in length, with numerous branchings, and having many spatulas per seta. Recently-taken high-quality scanning electron microscope (SEM) images of the hierarchical structures of a tokay gecko adhesive are shown in figure

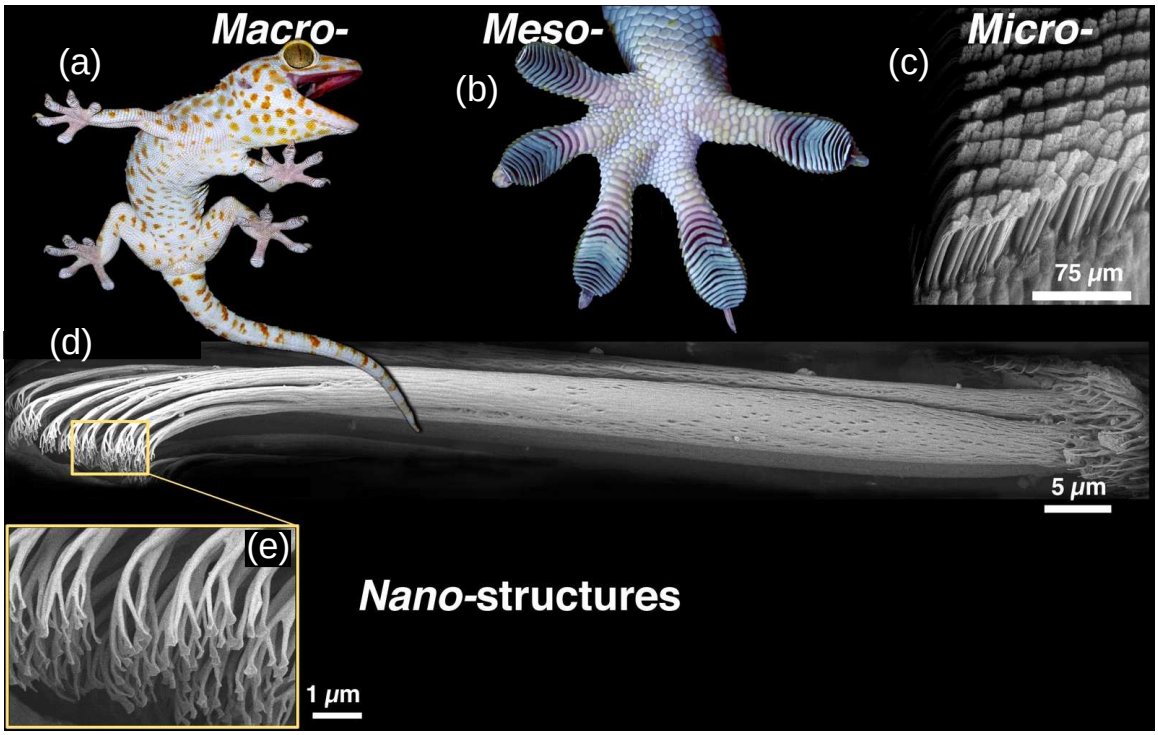

Figure 1.1: Tokay gecko and its hierarchical nano-micro structures. (a) Tokay gecko climbing a glass surface. (b) Gecko toes. Each toe has 10 - 20 lamellae. (c) Microscale array of setae on a lamella. (d) Single gecko seta. Length and diameter of a seta is about 100 μm and 5 μm respectively. (e) Nanoscale array of hundreds of spatular tips of a single gecko seta. Image by courtesy of professor Kellar Autumn in the Department of Biology, Lewis and Clark College, Portland, OR, USA

.

1.1. A tokay gecko sustaining its whole body on vertical glass with only one toe that is covered by the hierarchical structures is shown in figure 1.2.

In 2000s, by using a two-dimensional micro-electromechanical systems (MEMS) force sensor and a wire as a force gauge, Autumn *et al.* [10] reported the first direct measurements of single setal force. Measurements revealed that a seta is ten times more effective at adhesion than predicted from maximal estimates on whole

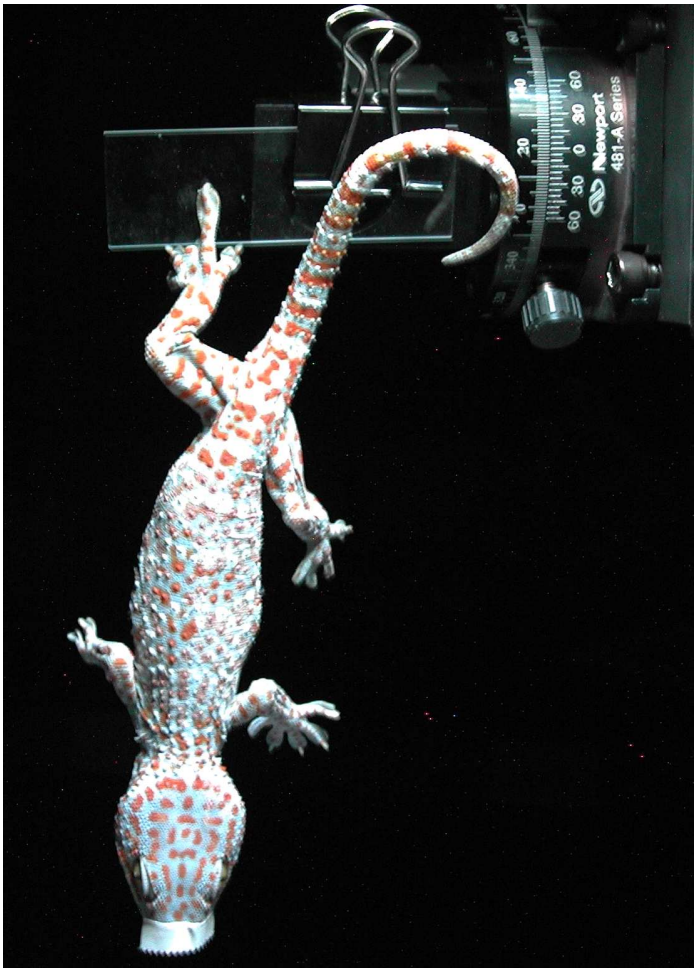

Figure 1.2: Tokay gecko sustaining its whole body on vertical glass using only one toe. Image by courtesy of professor Kellar Autumn in the Department of Biology, Lewis and Clark College, Portland, OR, USA

animals and suitably orientated setae reduced the forces necessary to peel the toe by simply detaching above a critical angle. Autumn *et al.* [12] also provided the first direct experimental evidence for dry adhesion of gecko setae by van der Waals forces, and rejected the use of mechanisms relying on high surface polarity, including capillary adhesion. A van der Waals mechanism implies that the remarkable adhesive properties of gecko setae are merely a result of the size and shape of the tips, and are not strongly affected by surface chemistry. However, interestingly, Huber *et al.* [26] reported measurements of the adhesion force exerted by a single gecko spatula for various atmospheric conditions and surface chemistries. In contrast to previous work [12], their measurements showed that humidity contributes significantly to gecko adhesion on a nanoscopic level.

After single setal force was measured and mechanisms for dry adhesion were suggested, unique properties of gecko adhesive have been revealed. Hansen and Autumn [25] demonstrated that gecko setae are a self-cleaning adhesive. Geckos with dirty feet recovered their ability to cling to vertical surfaces after only a few steps. Self-cleaning occurred in arrays of setae isolated from the gecko. Contact mechanical models suggest that self-cleaning occurs by an energetic disequilibrium between the adhesive forces attracting a dirt particle to the substrate and those attracting the same particle to one or more spatulae. Autumn and Hansen [8] also provided evidence that gecko setae are non-adhesive in their unloaded default state by comparing the water droplet contact angle of isolated setal arrays to the smooth surface of eye

spectacle scales of tokay geckos. Autumn *et al.* [6] found that gecko adhesion depends directly on shear force, and is independent of detachment angle. They introduced a new model, frictional adhesion, for gecko pad attachment and compared it to existing models of adhesive contacts. Recently, Gravish *et al.* [24] discovered that the energy required to detach adhering tokay gecko setae (Wd) is modulated by the angle of a linear path of detachment. They found that setae possess a built-in release mechanism. Setae acted as springs when loaded in tension during attachment and returned elastic energy when detached along the optimal path.

The question how the stiff β-keratin works as an adhesive was addressed by Autumn *et al.* [11]. They showed the effective elastic modulus of the adhesive on the toes of geckos made of β-keratin, a stiff material satisfies Dahlquist's criterion [18, 48] for tack since the gecko adhesive is a microstructure in the form of an array of millions of high aspect ratio setae. Peattie *et al.* [45] used a resonance technique to measure elastic bending modulus in two species of gecko and found no significant difference in elastic modulus between Tokay gecko (1.6 ± 0.15 GPa) and Ptyodactylus hasselquistii (1.4 ± 0.15 GPa).

The unique properties of natural gecko adhesive from the hierarchical nano-micro structures with stiff β-keratin are summarized in the followings.

- **High shear adhesion** A natural gecko setal array on a single lamella provides high adhesion [12, 25, 37] as much as 22 - 65 N/cm^2 depending on test methods and substrates. Required static adhesive force of a tokay gecko is 0.5 N/cm^2

considering the weight of 50 g and total pad area of 1 cm^2 [10]. The over-engineered gecko setal arrays make it possible for gecko to move dynamically as fast as 1 m/s [24] with small portion of setal contact with diverse surfaces.

- **Easy detachment** Gecko can detach their adhesive pads easily. Combined unique uncurling of toes [10] and detachment angle [6] helps gecko detach their toes from surfaces with minimal energy [24]. If gecko uses conventional tapes, it would be very difficult to run fast.

- **Directional adhesion** Tokay gecko setae are angled from surface normal about 45°. The angle provides directional adhesion [6] as well as normal compliance [11] enough for adhesion from stiff β-keratin. Tokay gecko setae adhere to surfaces when dragged along the setal direction and do not when dragged against the setal direction [6].

- **Self-cleaning** Gecko uses millions of hard-material based branched setal arrays (Young's modulus $E \sim 1.5$ GPa [11, 45]) to cling to and walk on virtually any surface while maintaining setal arrays clean enough to support the gecko's body weight [25]. The hard-material based setal arrays shed dirt particles while walking without any kind of liquid and grooming.

- **Durability** Geckos use their nano-micro structured adhesive for about two months between molts. The hard-material based setal arrays are durable enough for repetitive use between molts [25] in contrast to soft polymer based conven-

tional tapes which degrade easily after several repetitive uses.

As nano-micro technology develops, these unique properties of natural gecko adhesive have been unveiling and initiated a lot of scientists and engineers to make synthetic gecko tapes that have some of the novel adhesive properties.

1.2 Synthetic Gecko Adhesive

Natural gecko adhesive consists of sophisticated hierarchical arrays of setae as shown in figure 1.1. Due to challenges to make the same structures with the same material, many researchers have began to create simple structures with various dimensions and base materials.

Soft polymer (Young's modulus $\leq$ 10 MPa) is the mostly used material to fabricated gecko inspired synthetic adhesives (GSAs) [7] to enhance adhesion from adhesive smooth control. Sitti and Fearing [59] presented two fabrication methods using nano-indented flat wax surface and commercial nano-pore templates. They also proposed designing methods of parameters such as length, diameter, stiffness, density and orientation of hairs for non-matting and rough surface adaptability. Crosby *et al.* [17] proposed topographical patterns to selectively tune the adhesion of polymers. They demonstrated that properly designed, low-aspect-ratio posts can alter adhesion from 20% to 400% the value of conventional adhesion descriptors for non-patterned interfaces. They established general relationships that govern the interaction between

material properties, pattern length scales, and the control of adhesion.

Kim and Sitti [32] presented microfibers with flat spatulate tips as repeatable adhesives. Fabricated polyurethane fiber arrays by molding a master template using deep reactive ion etching and the notching effect demonstrated macroscale adhesion pressures up to 18 N/cm^2 and overall work of adhesion up to 11 J/m^2 on a 6 mm diameter glass hemisphere for a preload pressure of 12 N/cm^2, four times higher adhesion and five times higher overall work of adhesion than that of the flat surface. Gorb *el al.* [22] and Varenberg and Gorb [60] created mushroom-shaped fibrillar adhesive microstructure to improve the adhesive properties. Pull-off and peeling tests revealed that pull-off force and peel strength of the structured specimens are more than twice those of the flat specimens. Shearing tests of the fibrillar microstructure showed a stable and smooth sliding with a friction coefficient approximately four times lower than a control flat surface, which exhibited pronounced stick-slip motion.

Glassmaker *et al.* presented the unique structure consisting of protruding fibrils topped by a thin plate and showed an enhancement in adhesion energy of up to a factor of 9 over a flat control. They also showed that the geometry enhances adhesion because of its ability to trap interfacial cracks in highly compliant contact regimes between successive fibril detachments. Yao *et al.* [61] created the film-terminated fibrillar architecture with tilting the fibers to make the surface vertically more compliant and elastically anisotropic. The tilted fibrillar surfaces on a spherical glass lens showed significant directional anisotropy, demonstrating the directional

detachment and the sliding resistance.

Aksak *et al.* [1] fabricated microfibers with a controlled angle using optical lithography and polymer micromolding. Macroscale adhesion and overall work of adhesion of the microfiber arrays were measured and compared with their models to observe the effect of fiber geometry and preload. Murphy *et al.* [41] modified the angled polyurethane fiber arrays [1] by adding soft spherical and spatula shaped tips via dipping. Sphere and spatula tip fiber samples demonstrated increased adhesion with 10 and 23 times the maximum adhesion of the unmodified fiber sample, respectively. The sphere and spatula tip fiber samples also showed increased friction with 1.6 and 4.7 times the maximum friction of the unmodified fiber sample, respectively. The direction dependent friction of angled fibers was also investigated. Santos *et al.* [53] created a synthetic fibrillar stalks array which have angled faces at 45° and demonstrated directional adhesion up to approximately 1 N for a 3.9 cm^2 patch when pulled in the direction in which the stalks are angled in contrast to negligible adhesion along the other direction. The fibrillar stalks were used for a climbing robot, called StickBot [33].

On the other hand, hard (stiff) polymer (Young's modulus $\geq$ 1.5 GPa) has been used to achieve adhesion by fibrillating non-adhesive smooth surfaces. Geim *et al.* [21] made polyimide hairs microfabricated using electron-beam lithography and dry etching in oxygen plasma. The normal adhesive force was proportional linearly with sample size, and virtually independent of preload (for preloads $\geq$ 50 N/cm^2). The

macro scale 1 cm^2 patch was able to support 3 N in normal to the surface. Northen and Turner [43] creatred the multiscale integrated compliant structures (MICS) offering three levels of surface compliance. Nanoindentation adhesion tests showed adhesion force (~ 2 mN/cm^2) between the micro-fabricated samples and a rough 5 mm diameter aluminum flat punch. Kustandi *et al.* [35] presented wafer-scale polymer nanofibrillar structures using the combination of colloidal nanolithography, deep-silicon etching, and nanomolding. The whole 1 cm^2 adhesive pad was found to support 0.7 N in normal to the surface. They also presented cleaning properties of the sample using water.

Also, carbon nanotubes has been one of materials for GSAs. Zhao *et al.* [63] fabricated vertically aligned multiwalled carbon nanotube (MWCNT) arrays as a dry adhesive and demonstrated dry adhesion between MWCNT array surfaces and various target surfaces over millimeter-sized contact areas. The adhesive strengths were measured over 10 N/cm^2 in the normal direction and about 8 N/cm^2 in the shear direction with glass surface. Ge *et al.* [20] developed a synthetic gecko tape by transferring micropatterned carbon nanotube arrays onto flexible polymer tape. The gecko tape can support a shear stress of 36 N/cm^2 with 25 - 50 preload. Qu and Dai [50] demonstrated that the vertically aligned single-walled carbon nanotube (VA-SWNT) arrays have macroscopic adhesive force of 29 N/cm^2. The vertically-aligned dry adhesives showed fairly reversible semiconducting behaviors under load and an excellent thermal resistance.

1.3 Contribution

The goal of the work is to make easy attach, easy detach, mechanically controllable, and durable synthetic adhesive which is self-cleaning dirt particles. Specific contributions are listed below.

- **Sliding-enhanced shear adhesion** Sliding-enhanced shear adhesion is demonstrated with hard polymer microfiber arrays. Shear adhesion is tested and compared with natural gecko setal arrays. It is shown that shear adhesive force is independent of preload and sliding speed. Durability of the fibrillar adhesive is also discussed.

- **Self-cleaning of synthetic fibrillar adhesive** Self-cleaning of synthetic fibrillar adhesive is demonstrated for the first time. Shear adhesion is recovered as the contaminated fibrillar adhesive is used on a dry surface. It is shown that self-cleaning performance depend on size of dirt particles.

- **Directional adhesive with angled fiber arrays** Microfibers are angled from vertical axis and demonstrate anisotropic properties of the fibrillar adhesive. The microfiber arrays develop adhesion when dragged along fiber direction and do not when dragged against the microfiber direction. The angled fibrillar adhesives show adhesion with pure normal indentation tests in contrast to vertically aligned microfiber arrays.

- **Force measurement apparatus** A static shear, normal and peeling force

measurement apparatus is built up. Area of microfiber contact can be observed by illuminating glass substrate. A separate sliding force measurement apparatus is built up. Shear force can be measured and area of contact can be recorded whiling making a sample sliding on a substrate. A dual-axis force indenter is upgraded. Instead of spherical indenter, a sample can be mounted on a flat surface and can be tested on a flat substrate.

Chapter 2

Sliding-induced Adhesion of Stiff Polymer Microfiber Arrays

Gecko-inspired microfiber arrays with 42 million polypropylene fibers per square centimeter (each microfiber with elastic modulus 1 GPa, length 20 micrometers and diameter 0.6 micrometer) were fabricated and tested under pure shear loading conditions, after removing a preload of less than 0.1 N per square centimeter. After sliding to engage fibers, 2 square centimeter patches developed up to 4 newtons of shear force with an estimated microfiber contact area of 0.44 square centimeters. The control unfibrillated surface had no measurable shear force. For comparison, a natural setal patch tested under the same conditions on smooth glass showed about 7 times greater shear per unit estimated microfiber contact area. Similar to gecko fiber arrays, the synthetic patch maintains contact and increases shear force with sliding. The high

shear force observed (approximately 210 nN per fiber) suggests that microfibers are in side contact, providing a larger true contact area than would be obtained by tip contact. Shear force increased over the course of repeated tests for synthetic patches, suggesting deformation of fibers into more favorable conformations.

2.1 Introduction

Natural geckos have exceptional wall-climbing ability using their millions of micro/nano fibrillar structures. The gecko's keratin fiber arrays form a unique attachment mechanism which is non-adhesive by default [8], but can be easily engaged with low compressive preload and sliding to develop high shear force [10], and controllably released with low pull-off force [24]. These properties of natural gecko are critical for efficiently and reliably running up walls. In characterizing the behavior of a "directional" adhesive, it is refered to the tensile force (normal to a surface) and the shear force (parallel to a surface). It is important to note that the tensile and shear force can be strongly coupled, and may depend on both compressive preload (normal to surface) and engagement trajectories. In this chapter, the macro-scale behavior of a synthetic gecko patch is examined. As the whole patch is non-adhesive by default in the normal direction, the patch is tested under pure shear loading, where forces are constrained to be parallel to a surface.[1] Under shear loading, membrane buckling

[1]Pure shear loading with zero normal load or peeling moment was also used by Ge *et al.* [20] and Zhao *et al.* [63] to test patch behavior, and is well known in materials testing, e.g. (Antoniou & Bastawros [3]).

effects dominate behavior. In a separate paper, Schubert *et al.* [55] examined a micro-scale spherical indentation of a synthetic gecko patch which is fixed to a backing layer to avoid membrane buckling effects. Under combined shear and normal loading the patch demonstrates a *frictional adhesion* effect, whereby a normal tensile load can be supported only under conditions of an applied shear load.

There is increasing interest by researchers in understanding and fabricating Gecko-inspired Synthetic Adhesives (GSAs) [5, 7] using materials which range in hardness from soft polymers to carbon nanotubes (E $\sim 3 \times 10^5$ to 10^{12} Pa). Harder materials allow greater fiber packing density [59], and likely better resist wear and particle contamination. Recent work using soft polymer fiber arrays [32, 52, 22] has increased normal adhesion several times over the bulk material. Multiwalled carbon nanotubes (MWCNT) [63, 20] and low-aspect-ratio (length/diameter = 0.5 to 10) hard polymer stalks [21] demonstrated tensile adhesion but they require high normal compressive preload. Kustandi *et al.* [35] has recently demonstrated 0.7 N/cm^2 tensile adhesion with preload pressure of 1 N/cm^2 using 10:1 aspect ratio hard polymer microfibers (E $\sim$ 2.8 GPa).

Microfiber arrays have also demonstrated high friction forces (that is, high shear forces with normal compressive loads which engage fibers) such as Majidi *et al.* [39] with coefficient of friction $\mu > 5$ using polypropylene and Aksak *et al.* [2] with $\mu > 1$ using MWCNT. The shear force required a sustained normal compressive load and the samples did not show shear or tensile adhesion.

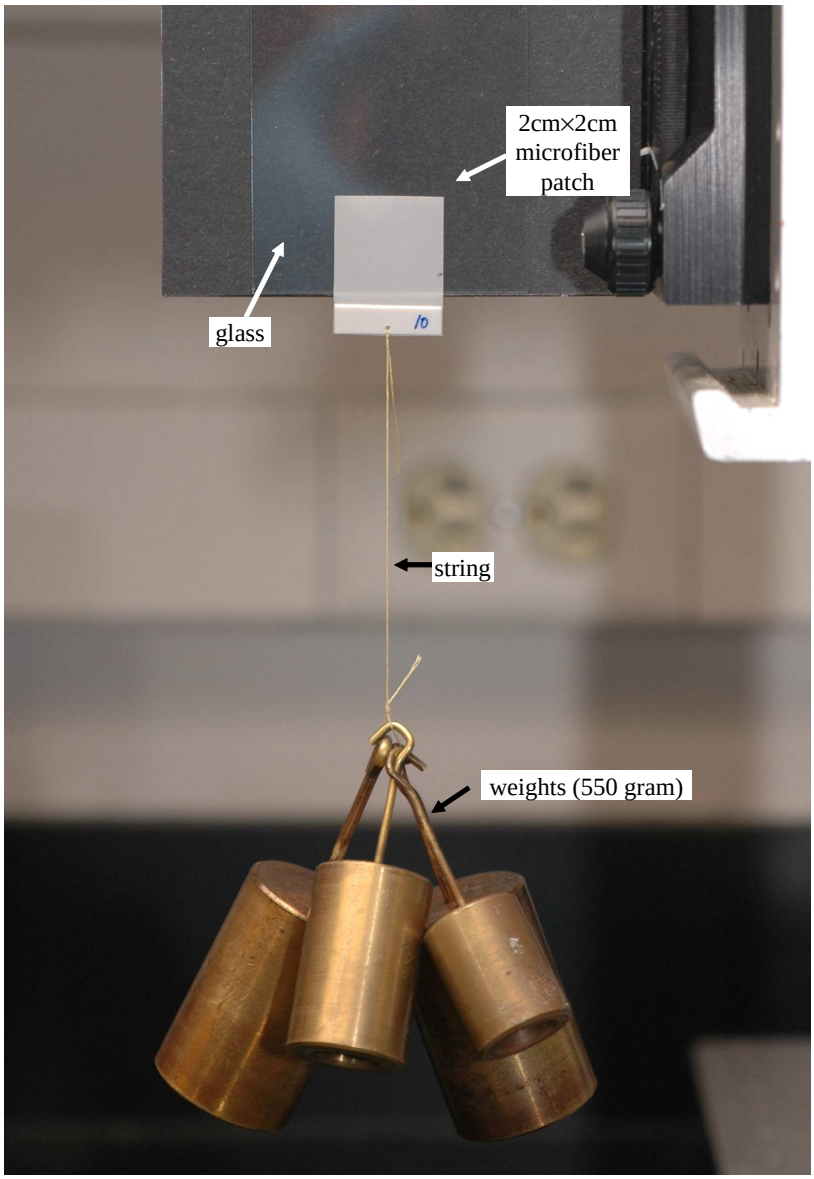

Figure 2.1: A 2 cm × 2 cm microfiber array patch holding weights (550 gram in total) on a vertical smooth glass slide without normal load.

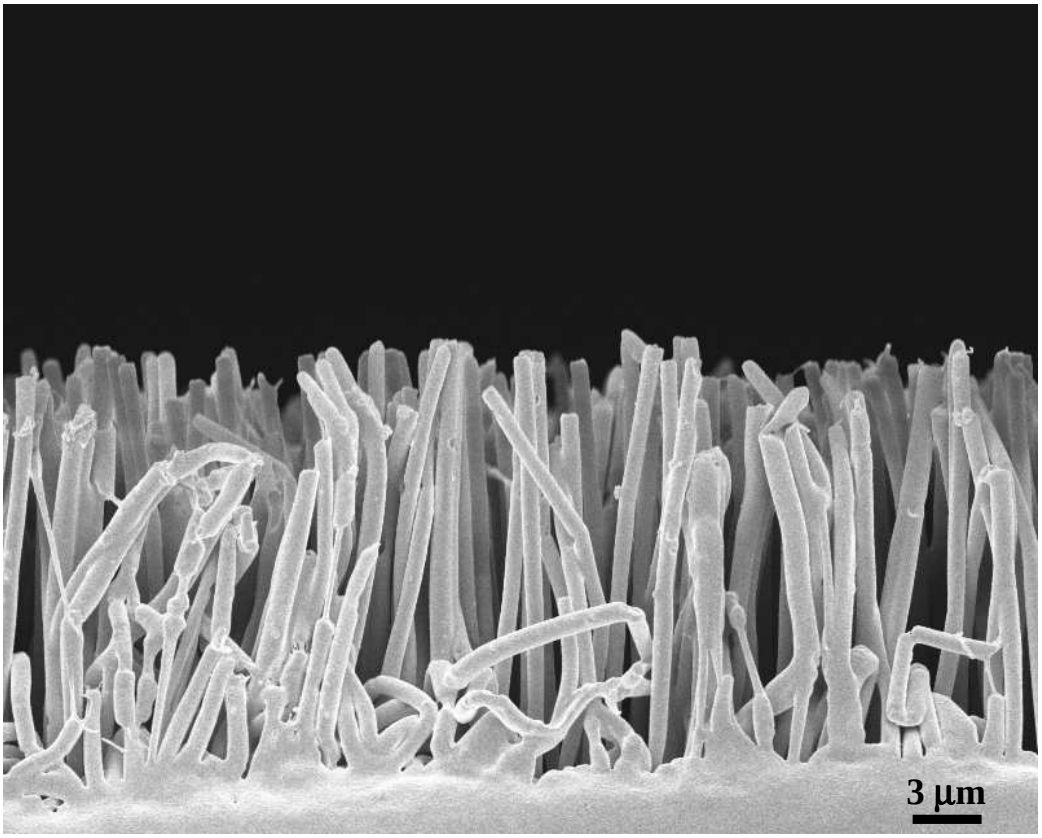

Figure 2.2: Scanning electron microscope(SEM) image of the microfiber array.

To simultaneously obtain high shear force and low tensile pull-off forces with a low initial compressive preload, An array of microfibers which make side contact with a surface [40] has been designed. In contrast, structures such as Geim *et al.* [21] and Kustandi *et al.* [35] use tip contact of fibers. It has been fabricated an array of 0.6 μm diameter polypropylene microfibers whose elastic modulus (E $\sim$ 1 GPa) and aspect-ratio ($\sim$ 30), are similar to natural tokay gecko setae with E $\sim$ 1.5 GPa [45, 11] and aspect-ratio $\sim$ 25 [51]. In contrast to Majidi *et al.* [39], these patches were fabricated with reduced backing curvature to enable microfiber engagement without sustained compressive normal loading. (The important effect of backing curvature on adhesion is discussed in Schubert *et al.* [56]) The flat backing samples with millions of microfibers per square centimeters (figure 2.2) show shear adhesion as demonstrated in figure 2.1.

In this chapter, it is directly compared the stiff polymer based microfiber adhesive to a natural gecko setal array under pure shear loading. The high elastic modulus material and vertical microfibers make the microfiber array intrinsically non-adhesive by default. (Angled microfibers as suggested by Sitti & Fearing [59] could be used to have an initially adhesive state.) It is shown experimentally that high shear adhesion can be induced by sliding displacement alone with minimal initial normal compressive preload, but can be easily detached in the normal tensile direction (low 90^o peel strength). It is also shown that the adhesion demonstrated in figure 2.1 does not depend on an internal viscoelastic property. Durability of some previous GSAs has

been a problem, e.g. Zhao *et al.* [63]. Tests of the polypropylene (PP) microfiber array showed an increase in shear adhesion force with repeated uses. In the Discussion, it is demonstrated that the measured shear stress in the estimated microfiber contact area of 9 N/cm^2 is consistent with microfibers in side contact with the surface.

2.2 Material and Methods

2.2.1 Material preparation

GSA samples were fabricated by casting a single layer of 25 μm thick polypropylene (TF-225-4, Premier Lab Supply Inc.) in a vacuum oven at 200°C into a 20 μm thick polycarbonate filter (ISOPORE, Millipore Inc.) containing 0.6 μm diameter pores. The polycarbonate filter was etched in methylene chloride, and resulting samples were rinsed in iso-propyl alcohol and air dried. Backing curvature was significantly reduced compared to previous microfiber arrays [39], increasing the number of microfibers in contact and adhesion. Using a fixed microfiber length, the microfiber diameter was selected to provide enough compliance while preventing microfibers from clumping. Control measurements were performed on processed 25 μm thick polypropylene film that underwent the same fabrication steps as the microfiber arrays, with the exception that no polycarbonate filter was applied. Both the microstructured samples and controls were cut into 2 cm $\times$ 2 cm squares. For some samples which demonstrated higher shear force than the limit of the force sensor, smaller areas (2 cm $\times$ 1.2 cm

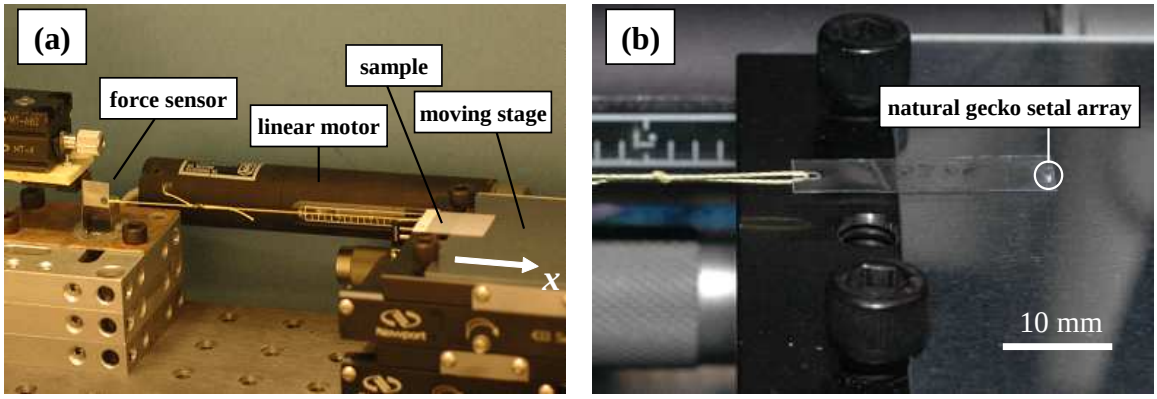

Figure 2.3: (a) Testing setup : shear force of a 2 cm × 2 cm synthetic microfiber array patch on a glass slide is being measured while the stage is driven in the x-direction by the linear motor. (b) Natural gecko setal array under shear load on same test setup.

and 2 cm × 0.8 cm) were used.

Natural gecko setal arrays were prepared by N. Gravish, M. Wilkinson and K. Autumn in the Department of Biology, Lewis and Clark College, Portland, OR, USA. Individual lamellae were isolated from tokay geckos. Each isolated lamella was fixed to the end of a 2.5 cm × 0.6 cm × 0.02 cm acetate strip using cyano-acrylate SuperGlue Gel. The areas of gecko setal arrays tested were 0.11 cm × 0.03 cm and 0.18 cm × 0.03 cm.

2.2.2 Measurement methods

Macro-scale shear adhesion tests during sliding with no normal compressive load were performed with the single axis force sensor system in figure 2.3(a) (More details can be found in appendix.) The system is composed of a stepper motor (TS Products model 2200) driven linear stage with a linear variable differential transformer (LVDT)

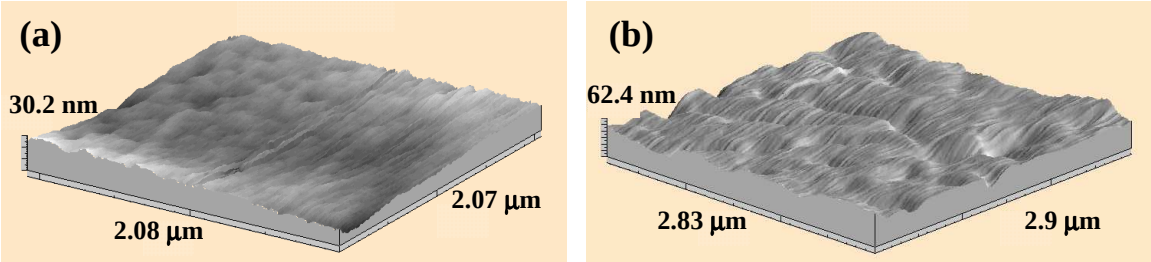

Figure 2.4: Surface roughness scanned by Atomic Force Microscope(Metrology AFM, Molecular Imaging Inc.). (a) Surface roughness of the glass substrate. Root mean square(RMS) = 3.3 nm. (b) Surface roughness of processed polypropylene control. RMS = 6.8 nm.

position sensor (MEPTS-9000, Techkor Instrumentation), and double cantilever force sensor [56]. The force sensors were calibrated with known weights. The force sensor for microfiber array samples had stiffness 10^5 N/m and resolution < 42 mN. A more sensitive force sensor (stiffness 3×10^4 N/m, resolution < 13 mN) was used for natural gecko setal arrays.

Each sample was connected to a force sensor using a string (Kevlar, Dupont) and was placed on a glass slide (Microscopes slides, Fisher Scientific) on top of the stage. The glass slide had surface roughness (root mean square(RMS) = 3.3 nm, figure 2.4(a)) and was cleaned using isopropanol to remove dust before using. Before shear testing, a normal preload pressure (< 0.1 N/cm^2) was applied by gloved finger to remove any possible initial curvature of the backing. A separate test showed that the preload used had a negligible effect on shear force. After the preload was removed, the stage was driven at constant speeds which ranged from 48 to 240 μm/s in the x-direction in figure 2.3(a). During testing, the normal stress due to weight of the patch

was less than 0.3 mN/cm^2. This normal stress is not needed to sustain shear stress as can be seen in figure 2.1. The gecko setal array under testing is shown in figure 2.3(b). While driving the stage, shear force and stage displacement were recorded by a 4 channel digital oscilloscope (TDS3014B, Tektronix).

Estimated microfiber contact area of samples was recorded by a camcorder (DCR-TRV520, Sony) using reflected white light through the back of the sample. This estimated microfiber contact area represents areas where microfibers may be touching the glass substrate. Due to backing membrane roughness, all microfibers in the bright contact area are not necessarily touching the glass.

2.3 Results

For both the microfiber array and natural gecko, shear force increased with sliding distance. The microfiber sample continued to function after 50 pure shear tests. In addition to durability, repeated sliding tests showed increase of maximum shear force of microfiber array samples.

As plotted in figure 2.5, shear force during sliding of a 2 cm $\times$ 2 cm microfiber patch increased as the patch was pulled on a smooth glass slide in the tangential (x) direction with no normal load. (Pressure due to weight of patch $<$ 0.3 mN/cm^2.) Pulling velocity for the stage was 120 μm/s. Effects of other preloads and velocities are presented later in this chapter. Initially, shear force increased as the stage moved for the first several millimeters and saturated at approximately 4 N shear force. From

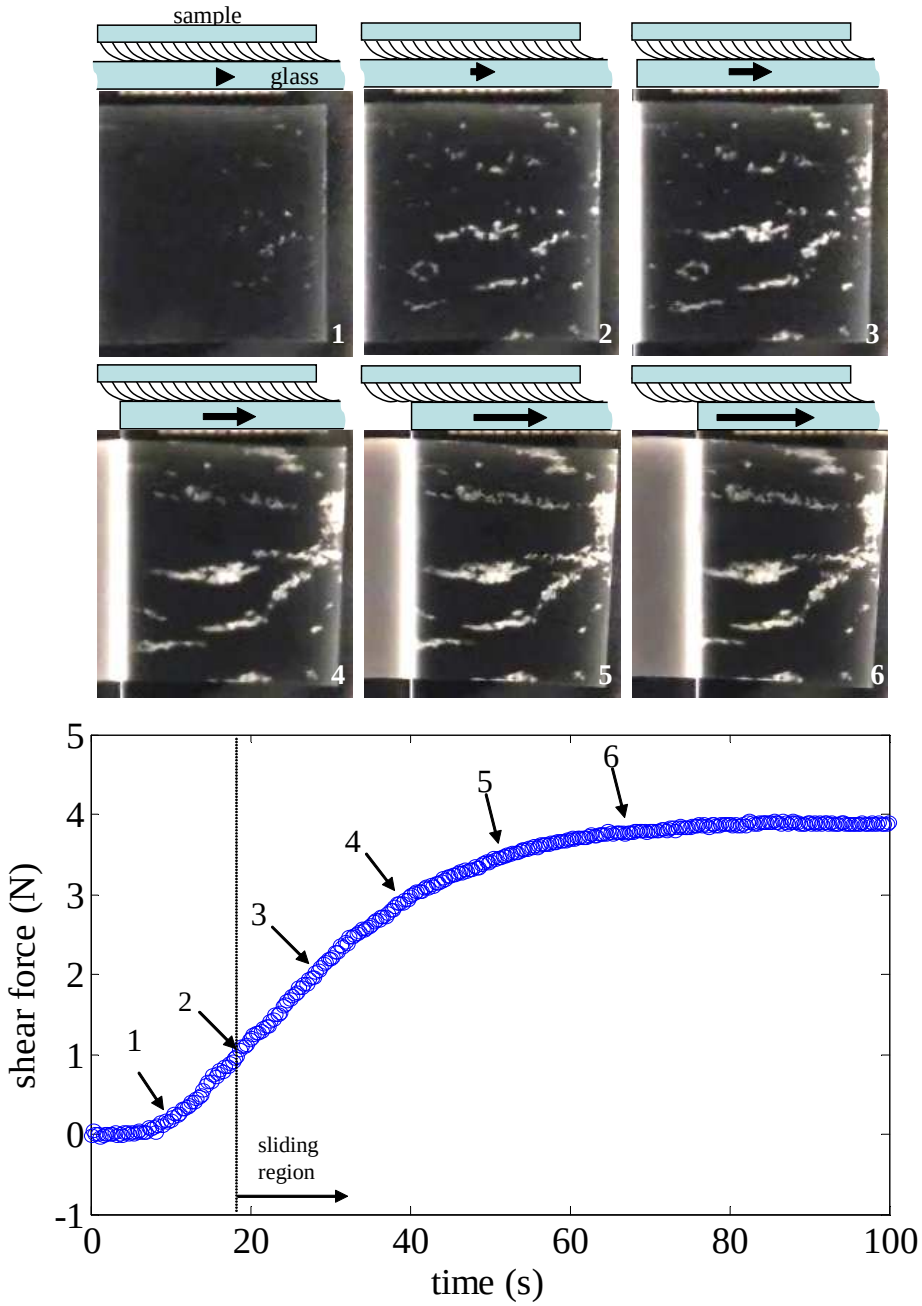

Figure 2.5: Shear force of a 2 cm × 2 cm synthetic microfiber array with zero normal load increased monotonically during tangential displacement (stage velocity $V_x = 120$ μm/s). Top images : Estimated microfiber contact area (bright spots) at indicated times. Shear force increases even as patch slides off glass. Estimated microfiber contact area is 11% of patch area, with possible buckling of membrane in dark (non-contact) regions.

examination of captured images, the sample did not slide until the shear force exceeded 1 N. Images 1-6 in figure 2.5 show that estimated microfiber contact area (bright spots) on glass increases as the synthetic microfiber patch slides. In image 1, the square patch placed on a glass slide had just several tiny contacting points after normal preload was removed. As the glass moved to the right (image 2-6), the initial contact areas grew. Even though the sample lost some overall overlap area (white square region in images 4-6) with the glass because the glass slid to the right, absolute shear force increased. The peak shear stress with estimated contact area fraction (estimate microfiber contact area (0.44 cm^2) / patch area (4 cm^2)) of 11% was 9 N/cm^2. The estimated microfiber contact area was determined by image processing (MATLAB R2006a, The MathWorks Inc.). The control (RMS surface roughness 6.8 nm, figure 2.4(b)), unstructured polypropylene, had no observable shear stress (< 0.3 mN/cm^2). The microfiber arrays have high shear adhesion but low normal adhesion. For example, only 3 ± 0.4 mN (mean$\pm$s.d., N = 5) of perpendicular force is required to peel the sample from glass. This corresponds to a 90^o peel strength of 0.15 ± 0.02 N/m.

Tests with a 0.18 cm $\times$ 0.03 cm natural gecko setal array with a gravitational compressive normal stress (< 50 mN/cm^2) showed similar sliding induced shear force and saturation (see figure 2.6). No external preload was applied. Pulling velocity for the natural gecko setal array was 120 μm/s. The top images in figure 2.6 show relative position of the natural setal array and glass under testing at indicated times.

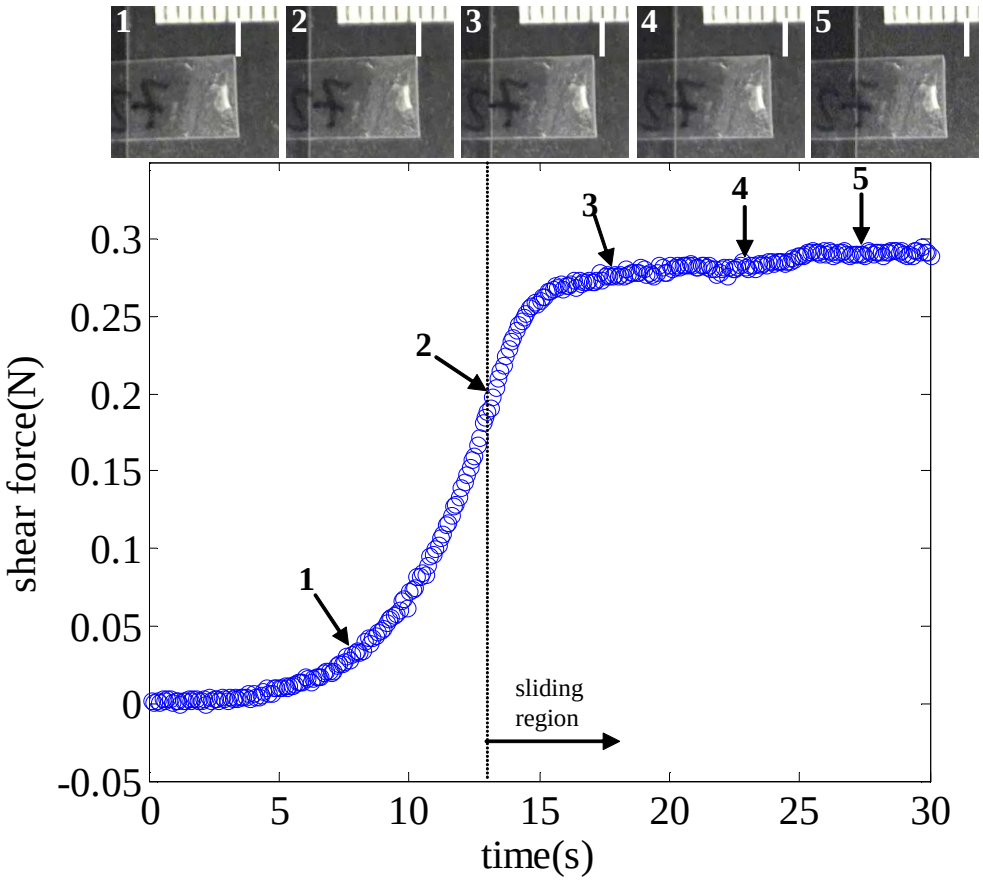

Figure 2.6: Shear force of a 0.18 cm × 0.03 cm natural gecko setal array with zero normal load during tangential displacement of the stage (stage velocity V_x = 120 μm/s). Top images : natural setal array under testing at indicated times. The captured images indicate that the sample actually began sliding at 13 sec due to compliance of the sensor system including the string.

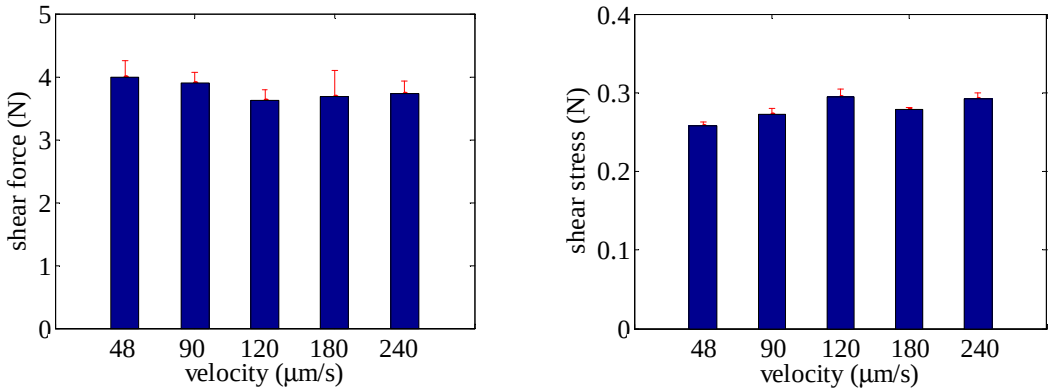

(a) Synthetic microfiber array.

(b) Natural gecko setal array.

Figure 2.7: Maximum shear force for various velocities. Each sample was tested 4 times at each velocity. Patch sizes of the synthetic microfiber array and natural gecko setal array are 2 cm $\times$ 0.8 cm and 0.18 cm $\times$ 0.03 cm respectively.

The images indicate that the gecko setal array started sliding after the shear force exceeded 0.2 N, and shear force approximately saturated after 200 μm displacement. Because of an initially slack string, stiffness of the force sensor system including a string is nonlinear. Linearized stiffness of the system is 250 N/m for 0 N $\sim$ 0.2 N and 1600 N/m for 0.2 N $\sim$ 1.6 N. Because of this low stiffness (250 N/m) for low load ($<$ 0.2 N), the gecko setal array did not slide until after 960 μm of stage movement, corresponding to 0.24 N shear force.

Velocity dependence was examined for both the synthetic adhesive and natural gecko setal array. Both samples were pulled four times at each velocity from 48 μm/s to 240 μm/s. Average and standard deviation of plateau force are plotted in figure 2.7. No drastic change in shear force with velocity was seen for microfiber arrays or the natural gecko setal array.

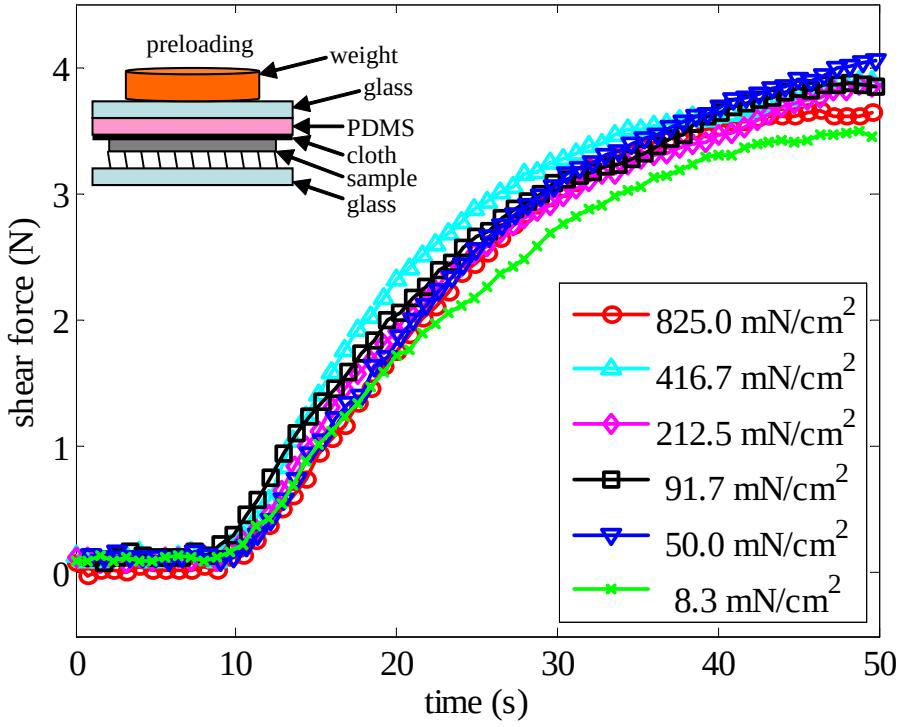

Figure 2.8: Shear force of a 2 cm $\times$ 1.2 cm microfiber array with different preloads. The sample was preloaded uniformly using a cloth, PDMS, glass and a weight.

In many GSAs, e.g. Gorb *et al.* [22] and Kim & Sitti [32] tensile adhesion force is a strong function of normal preload. Before shear testing, an approximately uniform preload was applied, and carefully removed before testing without disturbing the patch. A sheet of polydimethylsiloxane (PDMS) was used to distribute normal loading uniformly over a sample. A cloth (Technicloth, ITW Techwipe Inc) prevented soft PDMS sticking to a sample. After carefully removing the stack on a microfiber array patch, the patch was pulled at 120 μm/s. Figure 2.8 shows sliding induced shear adhesion for different preloads (8 mN/cm^2 $\sim$ 825 mN/cm^2), with no observable relation between preload and maximum shear force. In other tests, the microfiber array samples were gently preloaded ($<$ 0.1 N/cm^2) with a gloved forefinger for simplicity, since preload did not significantly affect maximum shear force.

Relaxation behavior of PP microfiber arrays and the gecko setal array was significantly less than pressure sensitive adhesives (PSAs) (Magic tape, Scotch®, 3M) whose adhesion relies heavily on internal viscous conformation. After engaging the array by sliding, the moving stage stopped at time 0 and shear force relaxation is plotted in figure 2.9(a) for a synthetic microfiber array and in figure 2.9(b) for a natural gecko setal array. After stopping, the microfiber array patch crept about 150 μm without leaving residue on the glass slide. Consequently, the shear force of the microfiber array decreased by 30% and then maintained a constant shear force. This experiment supports that shear adhesion of the synthetic patch does not depend on viscoelasticity of the material but sliding of microfibers on glass (see Discussion). Af-

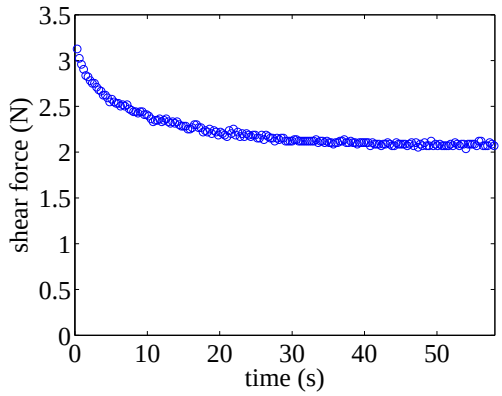

(a) Synthetic microfiber array.

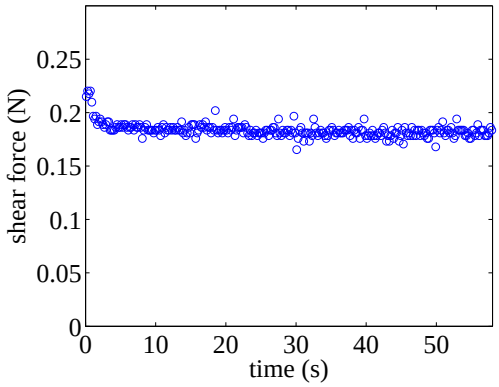

(b) Natural gecko setal array.

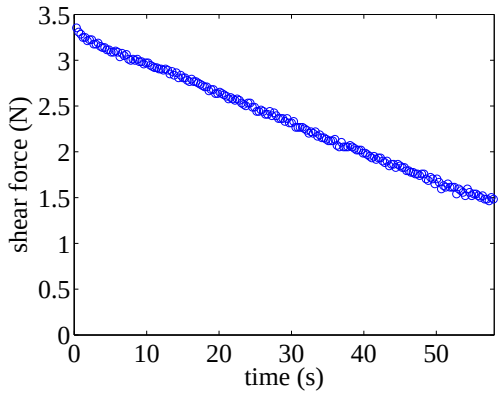

(c) Pressure sensitive adhesive.

Figure 2.9: Comparison of relaxation behavior of a microfiber array, natural gecko setal array and PSA after the stage stopped moving. Shear force of a microfiber array and natural gecko setal array decreased about 30% and 20% respectively and maintained constant level, while the PSA kept losing its shear force.

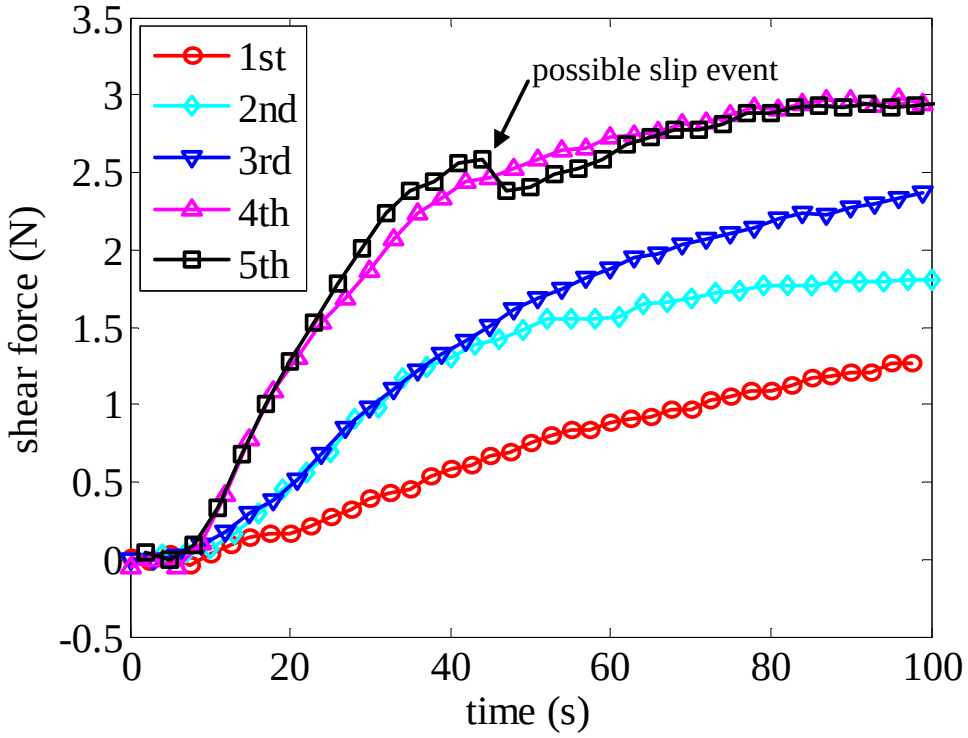

Figure 2.10: Shear force of a 2 cm × 2 cm microfiber array with repeated trials at 5 minute intervals after the array had relaxed for 4 days. For the sample, $V_x = 120$ μm/s.

ter stopping, as with the microfiber array, shear force of the natural gecko setal array also decreased by 20%, then maintained a constant level. In contrast to a microfiber array and natural gecko setal array, a 0.2 cm × 0.5 cm PSA adhered and did not slide on glass during loading. After stopping the stage at 0 sec, the PSA crept while leaving much soft polymer residue on the glass. Consequently, shear force kept decreasing as shown in figure 2.9(c).

Microfiber array patches survived more than 50 high shear tests without a reduction in shear force. Instead of a reduction in force, a training effect was observed

with repeated tests. As the sample was dragged repeatedly with zero normal load, maximum saturated shear force increased as shown in figure 2.10.

When shear force approached saturation, the sample sometimes slipped, presumably due to buckling of the thin backing of the patch as shown in the fifth test in figure 2.10. Shear force drops were also observed with natural gecko setal arrays at high load. For both materials, shear force recovered after slip events.

2.4 Discussion

Experimental results with centimeter-size microfiber arrays have shown several key GSA properties, including relatively strong shear adhesion with low peel strength, low normal preload for microfiber engagement, and durability over multiple attachment cycles. A microfiber side-contact model is discussed to explain the observed shear forces. Angling of the microfibers after sliding can be observed in microscope images, and is consistent with the increase in shear adhesion with use. Finally, it is compared the performance of various GSAs, and discussed how the behavior of the polypropylene microfiber array relates to tasks such as wall-climbing.

2.4.1 Shear adhesion induced side contact

The shear stress shown in figure 2.5 saturates at approximately 9 N/cm^2 per unit estimated microfiber contact area. With a microfiber density of $\rho = 42 \times 10^6$

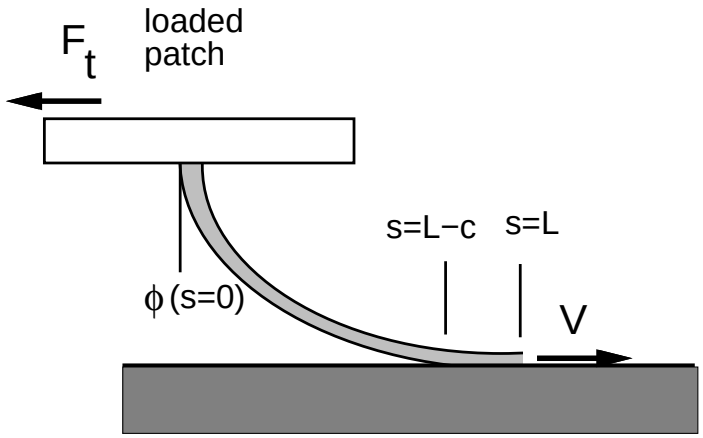

Figure 2.11: Elastica model of a microfiber under pure shear loading making side contact with a surface.

microfibers per square centimeter, this corresponds to an average shear force of approximately 210 nN per fiber. This shear force is much higher than predicted by Johnson-Kendall-Roberts (JKR) theory [30] for a spherical fiber tip[2]. For tip contact, the shear force can be estimated from $V_{tip} = \tau A_t$, where A_t is the true tip contact area, and τ is the interfacial shear strength (10 MPa for polypropylene on glass [49]). (Note that for hard polymers, the true contact area is very small compared to tip size.) The estimated shear force V_{tip} is only 33 nN for tip contact with $r = 0.3 \times 10^{-6}$ m microfiber radius, $E = 1$ GPa, and $W_{ad} = 30$ mJ/m^2, the work of adhesion of polypropylene on glass [23].

The tip contact model under estimates the measured shear force by a factor of

[2]The Tabor parameter [29] was calculated as 1.6 for a 0.3 μm radius microfiber tip. This is closer to the JKR region ($> 3 - 5$) than the DMT region (< 0.1), and hence the JKR model of contact was used.

6. However, it is observed that the measured shear force on the microfibers is high enough to cause the initially straight microfiber to have *side contact* (figure 2.11) with the glass. Side contact gives rise to much larger true contact areas than are predicted for tip contact. A side contact model is used to provide upper bounds on microfiber shear force. Previously, the side contact model was used to explain the normal adhesion of carbon nanotubes, silicon nanowires, and other high-aspect-ratio nanoscale fibers [40, 38]. Specifically, side contact is stable when the surface forces exceed the elastic restoring forces in the deformed fiber. Bending is aided by the shear load V applied to individual microfibers as the sample is dragged along a substrate.

To model the large deformations required for side contact, the fibers are treated as elastic rods. In their natural (undeformed) configuration, the microfibers are straight. During sliding each microfiber is loaded by a shear force $V = V_s$. $v = v(s)$ denotes the lateral deflection of a microfiber of length L caused by a shear load V acting on the tip. The coordinate s represents the arc length from the microfiber base. The elastica solution corresponds to the function $\phi = dv/ds$ that satisfies the ordinary differential equation

$$EI\phi'' + V_s \cos\phi = 0\,, \tag{2.1}$$

where the prime denotes the derivative with respect to s, E is elastic modulus, and I is cross sectional moment of inertia.

Letting c denote the length of side contact, it follows that $\phi = \pi/2\,\forall s \in [L-c, L]$. Along the segment $s \in [0, L-c]$, ϕ is the solution to (2.1) along with the boundary

conditions $\phi(0) = 0$ and $\phi(L-c) = \pi/2$. The unknown c is determined by the natural boundary condition [38]

$$\frac{1}{2}EI\{\phi'(L-c)\}^2 = \omega\,, \tag{2.2}$$

where ω is the energy of adhesion per unit length of side contact. From Majidi *et al.* [40]

$$\omega = 6\left\{\frac{(1-\nu^2)r^2{W_{\text{ad}}}^4}{\pi E}\right\}^{1/3}\,. \tag{2.3}$$

Due to surface roughness of the fiber, the actual energy of adhesion per unit length is likely to be significantly lower than predicted [47]. The length of stable side contact c^* is determined numerically by simultaneously solving equations (2.1), (2.2), for $V = V_m(c)$, where V depends on contact length. The analysis predicts stable side contact under pure shear loading. The length of stable side contact is approximately $c^* = 9.5$ μm.

Two bounds are considered for the maximum shear force, spontaneous fracture of the entire interface (V_1) and elastic peeling (V_2). Both bounds will over estimate shear force, as they ignore surface roughness, and possible interference between microfibers or backing membrane buckling.

If sliding occurs only after spontaneous fracture of the entire interface, then the strength of the individual microfiber contact will be proportional to the total true area of side contact, cb, where

$$b = 8\left\{\frac{(1-\nu^2)r^2W_{\text{ad}}}{\pi E}\right\}^{1/3} \tag{2.4}$$

is the width of contact [40]. For the PP microfiber parameters, $b = 74$ nm. Thus, an upper bound on the shear force for a single microfiber in side contact is

$$V_1 = \tau c b. \tag{2.5}$$

From above, the predicted shear force V_1 is 7 μN, greatly exceeding the 210 nN shear force estimated from experiment. (Using 210 nN shear force, the estimated true contact area per microfiber is only 2.1×10^{-10} cm^2, and a cm^2 of patch has estimated true contact area of 0.009 cm^2, only 0.9% of the patch area.)

Contact shear failure can also result from the stretching of the fiber on the surface, which corresponds to the elastic term from the Kendall peel model [31] at low peel angle. Converting from the rectangular strip in the Kendall peel model to a cylinder in side contact, V_2 is obtained by

$$V_2 = \sqrt{2E\pi r^2 \omega}\,. \tag{2.6}$$

The upper bound V_2 for low-angle peeling is 970 nN, again greatly exceeding the average experimental value.

As mentioned above, surface roughness of the microfibers will reduce the effective work of adhesion, partially explaining the lower measured shear force. In addition, the estimated side contact length $c^* = 9.5$ μm for an isolated microfiber is not likely to be achieved in a structure with average fiber-to-fiber spacing of 1.5 μm. Hence, interactions between neighboring microfibers may prevent an average microfiber from being in complete side contact.

In contrast to sliding shear force, the tensile pull-off force is quite low, as the microfiber will spontaneously transition to tip contact once the shear load is removed. In tip contact, the normal pull-off force $F_{JKR} = \frac{3}{2}\pi r W_{ad} = 42$ nN. In pull-off in the normal direction, height variation of the microfibers (approximately uniform distribution, 17-20 μm), combined with low vertical compliance in tension, drastically reduces pull-off force [39]. In contrast, since side contact length c^* is much greater than height variation, the shear force is much less dependent on microfiber height variation. Hence the high shear adhesion and low normal adhesion force is consistent with the side contact elastica model.

2.4.2 Sliding and Viscoelastic Effects

While the side contact elastica model explains high shear force, it does not directly explain sliding enhanced shear adhesion. Compared to microfiber length (20 μm), a long sliding distance (5000 μm) was required to reach maximum shear force (4 N) as shown in figure 2.5. The long sliding distance required for maximum shear force can be partially explained by a growing estimated microfiber contact area being balanced by buckling of the thin polypropylene backing. As shown in image 1 in figure 2.5, initially only several points are touching the glass, presumably due to natural curvature of the backing and height variation of fibers. As the array slides, a greater number of microfibers are engaging and the backing begins buckling. Thus, estimated microfiber contact area and buckled area are competing during sliding, which leads to shear force

increasing and then saturating.

In our experiments, the natural gecko patch reached maximum shear force after only 200 μm of sliding, with no normal preload. This is comparable to the $\approx$ 100 μm distance seen by Autumn *et al.* [6], who used a relatively large normal preload 1 N/cm^2 before sliding, possibly explaining the shorter distance for full fiber engagement. Although there is no direct observations of estimated microfiber contact area for the natural gecko patch during sliding, it is speculated that buckling may be less significant. This could be due to the gecko lamellar structure, the patch being mounted to a relatively thick (0.02 cm) acetate strip, as well as the relatively small patch size.

Tests with different dragging velocities on the synthetic and natural patches in figure 2.7 are consistent with shear force increasing with sliding distance, not on sliding velocity, in the range from 48 $\sim$ 240 μm/s. In the separate paper, Schubert *et al.* [55] tested the velocity range from 5 μm/s to 100 μm/s with similar results. It is noted that the basic shear force model in equations (2.5) and (2.6) has no velocity dependence, although it cannot be ruled out velocity dependent effects at higher velocities.

Relaxation tests support that shear adhesion of microfiber arrays does not depend on an internal viscoelastic property of the material, but rather the surface interactions between PP microfibers and glass. In fact, the shear force drop in figure 2.9(a) can be explained by a combination of creep relaxation in the force sensor, and sliding of the

microfibers under tension after stage motion stopped. The force sensor was directly connected to the stage by a string, and stiffness was measured as 4.5×10^3 N/m. The stage was moved and stopped with the string under tension, and measured force relaxed from 2.79 N to 2.58 N. Sliding of the microfiber patch after stopping the stage was about 150 μm which corresponds to about 0.68 N shear force drop due to sensor and string stiffness. Thus, most of the force drop (about 1 N) in figure 2.9(a) can be explained by relaxation (0.21 N) of the force sensor/string combination and sliding (0.68 N) of microfibers.

In contrast, the PSA (0.1 cm^2) did not slide on the glass and shear force increased rapidly while the stage moved, but the PSA relaxed slowly after stopping due to viscoelasticity of the soft polymer. In addition, there was much soft polymer residue on the glass after testing with the PSA, which indicates cohesive failure rather than surface sliding between the PSA and glass. After experiments with the PP microfiber array and natural gecko setal array, no residue was found on the glass. These comparisons support that the viscous deformation typical of detaching PSAs does not seem to occur in the gecko setal array [24] or in our microfiber array. Thus, our microfiber array is free from material degradation as opposed to PSAs which lose viscoelastic energy from internal friction processes such as cavitation and fibrillation [16]. The low viscoelastic losses of the PP GSA are consistent with the observation that the microfiber array has high shear adhesion but has low peel strength, as minimal energy is dissipated during peeling.

2.4.3 Preload independence

Preload was not an important factor for the saturated shear force as shown in figure 2.8. As shown in the top left image in figure 2.5, the initial estimated microfiber contact area is very small without sliding displacement, even after application and removal of a compressive preload. After the preload is removed, a small number of microfibers in a few regions may be adhering to the glass. Higher and lower preloads do not significantly change initial estimated microfiber contact area. It is observed that a compressive preload apparently flattens the patch uniformly against the surface, removing any initial curvature. The maximum preload of 0.825 N/cm^2 is less than the load of 1.6 N/cm^2 estimated by Majidi *et al* [39] to buckle all fibers, hence not all microfibers are making contact with the glass during preload. In addition, the image of the estimated microfiber contact area shows no evidence of microfiber engagement over the whole patch after preload is removed, which is consistent with the non-adhesive default state of the vertical fibers.

A uniformly increasing estimated microfiber contact during sliding helps to prevent contact concentrations which can lead to the backing buckling. Thus, slight touching the samples with a gloved finger was enough preload for high shear adhesion. It is noted that the microfibers are only stably in side contact with a shear load applied; the normal preload will not engage microfibers in side contact, and when preload is removed, microfibers will return to the default vertical state. Hence, the independence from compressive preload further supports the side contact model.

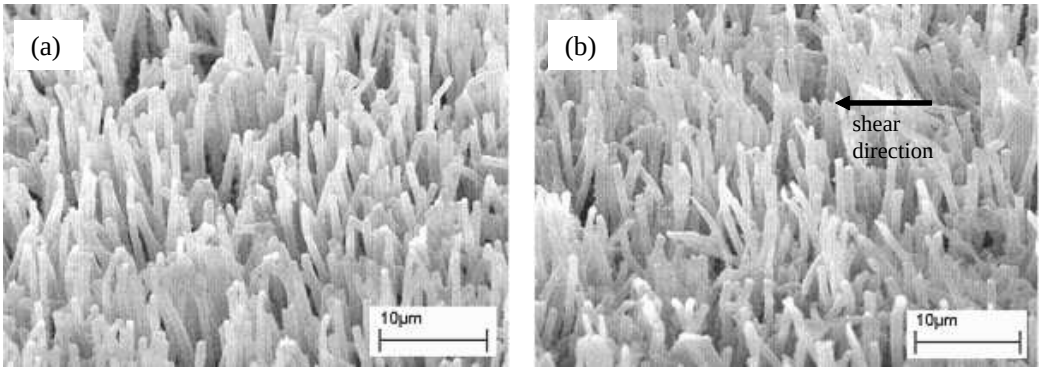

Figure 2.12: SEM images of microfibers. (a) Before testing. (b) After shearing more than 50 times. The arrow indicates shearing direction. Only a few microfibers show deformation. Images in (a) and (b) were taken from different spots.

2.4.4 Durability

To examine contamination or wear, scanning electron microscope (SEM) images of an unused (see figure 2.12(a)) and a used sample (see figure 2.12(b)) which was shear-tested more than 50 times were taken. Contamination or obvious wear was not visible although there are some microfibers plastically deformed along the shear direction due to repeated high shear loadings.

Shear adhesion of the samples increased as tests repeated, as shown in figure 2.10. Enhanced performance is likely caused by angling of the fibers, which makes the microfibers more compliant in the normal direction [59] and reduces height variation. Examination with an optical microscope showed that microfibers were angled after repeated testings as shown in figure 2.13. High shear loading angled some of microfibers (presumably microfibers engaged with surface) but did not angle all fibers uniformly. The angling was not permanent, and microfibers recovered to near vertical

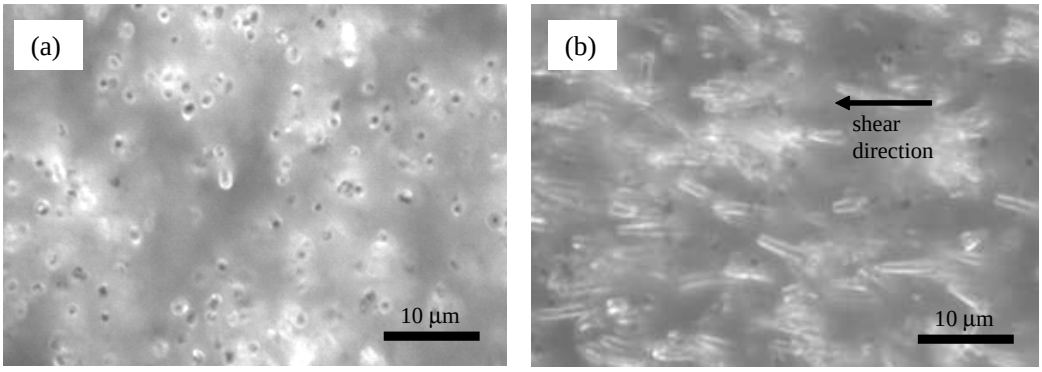

Figure 2.13: Top view of microfibers through an optical microscope. (a) Vertical fibers. (b) Bent microfibers within 10 minutes after loading high shear force. The arrow indicates shearing direction. Images in (a) and (b) were taken from different spots.

after several hours when unloaded. Thus, developing a fabrication method for uniformly and permanently angled fibers will be an interesting research topic. Although photolithographic methods have been used to make 25 μm diameter angled fibers [1], the 0.6 μm microfiber diameter used here may be a challenge for lithographic methods.

2.4.5 Implications for climbing robots and comparison to other GSAs

Pure shear tests at the whole-patch scale showed several properties which are important for climbing robots. The peel strength of 0.15 N/m is low enough for easy detachment during vertical running. Shear force increased with sliding distance, which is critical for arresting slip (which could lead to a fall). For both natural and

synthetic microfiber arrays, shear force recovered after slip events. It is likely that these displacement dependent forces will be important in stabilizing dynamic wall climbers [9].

The polypropylene (PP) based microfiber array described in this paper has similar stiffness and aspect ratio to natural tokay gecko. Although actual length ($\sim$ 20 μm) and diameter ($\sim$ 0.6 μm) of the PP microfibers are less than those of natural tokay gecko's setae, the unbranched PP microfibers have very close dimension to natural anolis (length $\sim$ 12 μm, diameter $\sim$ 0.5 μm) [51]. It is expected that the hard material used in the PP microfiber arrays will be important for long term durability and eventual self-cleaning properties which will be difficult with a softer polymer.

Table 2.1: Comparison of other adhesives. (a) This paper. (b) Santos *et al.* [52]. (c) Gorb *et al.* [22] and Varenberg & Gorb [60]. (d) Ge *et al.* [20]. (e) Kim & Sitti [32]. (f) Kustandi *et al.* [35]. PP:Polypropylene, PU:Polyurethane, PVS:Polyvinylsiloxane, MWCNT:Multiwalled carbon nanotube.

	tokay gecko	(a)	(b)	(c)	(d)	(e)	(f)
aspect-ratio	25	30	2.63	2.5	50000	4.4	10
length(μm)/diameter(μm)	100/4	18/0.6	1000/380	100/40	400/0.08	20/4.5	2.5/0.25
material	β-keratin	PP	PU	PVS	MWCNT+PSA	PU	parylene
elastic modulus (GPa)	1.5	1	0.0003	0.003	1000	0.003	2.8
sample area (cm^2)	0.0054	2	4	0.066	0.16	0.03	1
preload pressure(N/cm^2)	< 0.05	< 0.1	0.06	0.2	50	12	1
shear stress (N/cm^2)	55	2	0.3	N.A.	36	N.A.	N.A.
unstructured shear (N/cm^2)	0	~ 0	N.A.	2.27	N.A.	N.A.	N.A.
normal w/o shearing (N/cm^2)	0	~ 0	~ 0	6.06	5	18	0.7

It is worthwhile to compare the performance of the PP microfiber array to other recent work in GSAs as summarized in table 2.1. A particularly important property for a gecko-like adhesive is that one should be able to obtain a high shear force (useful for climbing) yet a low normal force (for easy detach). One can note that a conventional PSA can be used to obtain both high shear adhesion and high normal pull-off forces on glass. In addition, a low normal preload is desired for ease of engagement during running. Of the GSAs in table 2.1, only the reported PP microfiber array and the soft polyurethane (PU) structures of Santos *et al.* [52] show the desirable directional adhesive and low preload properties in a macroscale patch. These PU based angled stalks with a sharp tip have negligible normal adhesion without shear load even though the material is soft. It is interesting to note that poly vinyl siloxane (PVS) based mushroom shaped stalks [22, 60] have high normal adhesion (6.06 N/cm^2) without shear load but become non-adhesive with shear loading because the mushroom-shaped tips rotate away from the contacting surface.

2.5 Conclusion

Gecko inspired synthetic microfiber arrays were fabricated with a non-tacky hard polymer. As with natural gecko setal arrays, the fabricated microfiber array shows increasing shear force as a function of sliding distance on smooth glass. This unique property provides stability of the detachable adhesive (robust to a shear disturbance or vibration). Comparisons with PSA supports that shear force from the microfiber

array does not depend on viscous creep, thus, low energy detachment is possible. The durable microfiber array was able to hold as great as 4 N in shear with a 2 cm^2 nominal patch area when the array slid 1 cm and had shear stress greater than 9 N/cm^2 for the estimated microfiber contact area, approximately 15% of the natural gecko lamella patch tested. The high shear adhesion force is due to side contact, which could substitute for complicated spatula structures on smooth surfaces. The PP microfiber array has sufficient shear adhesion for small climbing robots, and has the unique property that performance improves with use, likely due to microfiber deformation.

Chapter 3

Contact Self-cleaning of Synthetic Gecko Adhesive from Polymer Microfibers

Natural gecko toes covered by nano-micro structures can repeatedly adhere to surfaces without collecting dirt. Inspired by geckos, a high aspect-ratio fibrillar adhesive was fabricated from a stiff polymer and self-cleaning of the adhesive was demonstrated during contact with a surface. In contrast to a conventional pressure-sensitive-adhesive (PSA), the contaminated synthetic fibrillar adhesive recovered about 33% of the shear adhesion of clean samples after multiple contacts with a clean, dry surface.

3.1 Introduction

Conventional pressure-sensitive adhesives (PSA) use soft viscoelastic polymers (Young's modulus < 100 kPa measured at 1 Hz [18, 48, 11]) to make intimate contact with surfaces to achieve high adhesion. However, soft polymers tend to collect dirt and lose adhesion with repeated use. In contrast, a gecko uses millions of keratinous nano and microhairs (Young's modulus $E \sim 1.5$ GPa [11, 45]) to cling to and walk on virtually any surface. These hairs shed dirt particles during contact to the adhesive, maintaining its natural adhesive clean enough to support the gecko's body weight [25].

A key factor in the self-cleaning ability of gecko structures is the nonadhesive default state exhibited by the gecko fibers [8]. To adhere, the fibers need to be dragged to expose the spatular tips, increasing the contact fraction by approximately 7.5-fold [8]. In contrast to the well-known *lotus effect* [13], in which particles are removed from a non-adhesive and highly hydrophobic surface by water droplets, gecko setae self-clean particles during use, even on dry surfaces. We restrict our discussion here to the self-cleaning of adhesives on dry surfaces during use. Natural gecko setae are the only previously reported self-cleaning adhesive on dry surfaces.

Recently, gecko-inspired synthetic adhesives (GSAs) [7] have been fabricated using soft polymers (Young's modulus ≤ 10 MPa) [59, 22, 32, 41, 17, 42] or hard polymers [21, 35, 43, 56] (Young's modulus ≥ 1.5 GPa). Also, arrays of carbon nanotubes (CNT) have been used to achieve adhesion [63, 20, 50]. Fibrillar adhesive cleaning

has been demonstrated using water [35, 57] and mechanical vibration [57]. Superhydrophobicity may lead to the cleaning of fibrillar adhesive by water [15]. However, no synthetic adhesive has demonstrated self-cleaning on dry surfaces during use, one of the important advantages of a gecko-inspired adhesive over conventional pressure-sensitive adhesives.

Autumn [4] has identified seven benchmark properties that are characteristic of geckolike adhesives, which are (1) anisotropic attachment, (2) high adhesion coefficient, (3) low detachment force, (4) material-independent adhesion, (5) self-cleaning, (6) anti-self-adhesion, and (7) non-sticky default state. Although properties (1)-(4) and (7) have been previously demonstrated [37, 34] in a single material, this chapter reports the first geckolike microfibrillar material that also demonstrates self-cleaning during contacts.

To create a self-cleanable adhesive, we fabricated high-aspect-ratio fibrillar arrays from polypropylene (Young's modulus $E \sim 1.5$ GPa, measured with a Sintech tensile tester 2/S, MTS Systems). In previous work, these hard-polymer-based fibrillar materials have shown unique adhesion properties, similar to gecko setae, including sliding enhanced shear adhesion [37] with low peeling force and frictional adhesion [6] with a spherical indenter [55]. In this chapter, a similar contact "step" protocol is used similar to that used for natural gecko setal arrays [25] to demonstrate self-cleaning of the synthetic fibrillar adhesive. The self-cleaning synthetic adhesive should be useful in a variety of applications where conventional adhesives can be easily contaminated.

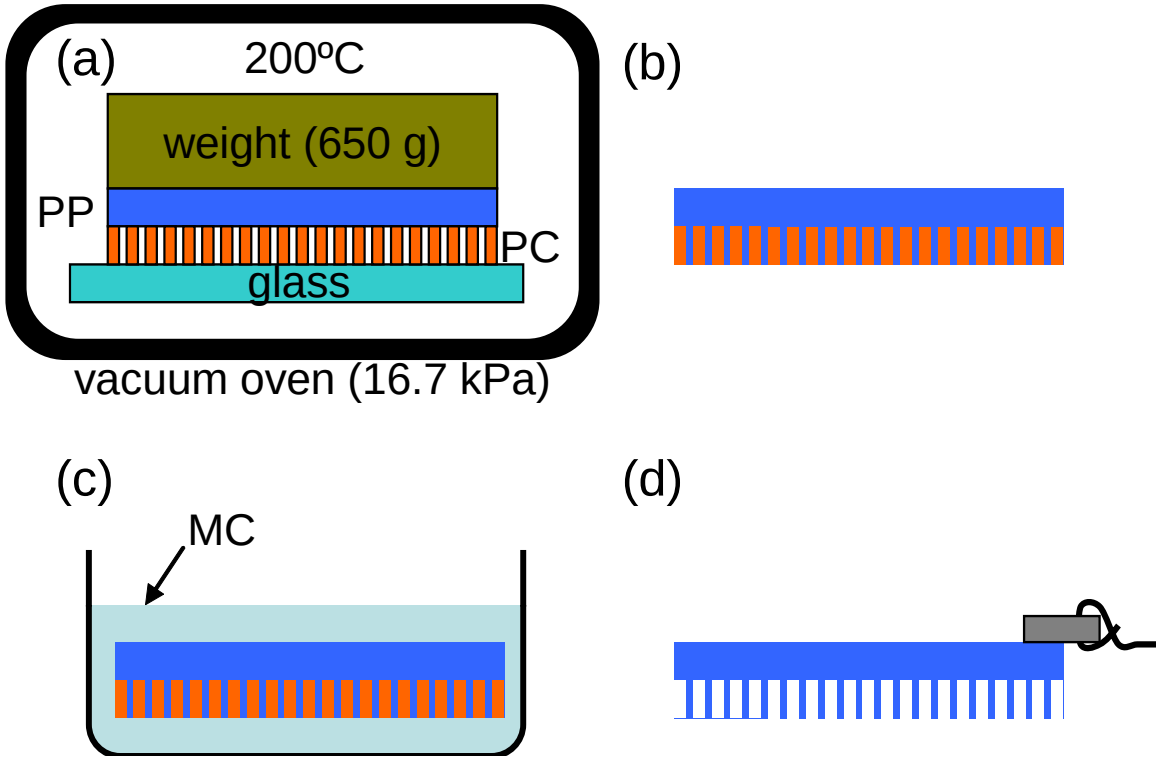

Figure 3.1: Schematic illustration of the fabrication process of polypropylene fibrillar adhesives. (a) A polypropylene (PP) film was casted in a vacuum oven into a polycarbonate (PC) template for 28 min. (b) The casted PP film and PC template cooled down to room temperature for 30 min. (c) The PC template was etched completely for 10 min in a first bath and 5 min in a second bath of methylene chloride (MC). (d) The resulting sample was rinsed in isopropyl alcohol and air dried. A string-connected load bar was attached to distribute the pulling force evenly.

3.2 Materials and Methods

3.2.1 Materials

The fibrillar adhesives were fabricated by casting a single layer of 25-μm-thick polypropylene (PP) film (TF-225-4, Premier Lab Supply Inc.) in a vacuum oven at 200°C into a 20-μm-thick polycarbonate (PC) track-etched membrane filter (ISO-

PORE, Millipore Inc.) containing 300-nm-radius pores as illustrated in figure 3.1(a). Using a fixed microfiber length, this microfiber radius was selected to provide bending compliance while preventing microfibers from clumping. The polycarbonate filter was etched completely for 10 min in a first bath and 5 min in a second bath of methylene chloride, to release the polypropylene fibrillar surface and film. The resulting samples were rinsed in isopropyl alcohol and air dried. The polypropylene film contains approximately 42 million microfibers per square centimeter with average length and radius of the microfibers 18 μm and 300 nm, respectively. The microstructured polypropylene film was cut into 2 cm $\times$ 2.5 cm rectangles using a razor blade, and 2 cm $\times$ 0.5 cm $\times$ 0.05 cm load bar with a small hole in which a string goes through was attached to distribute the pulling force uniformly.

To simulate contamination with dirt particles, microspheres with a mean radius 1.15 μm (gold powder, spherical, radius $\leq$ 2.5 μm, Alfa Aesar) were applied to cover the whole area of fibrillar adhesives and conventional pressure-sensitive adhesives by freely dropping microspheres from about 5 cm above the adhesives. Au microspheres were supplied in dry powder form with only weak clumping. Au microspheres were applied uniformly with similar density on the PSA and fibrillar surfaces by gravity, without applying any contact force.) After application, the adhesives were gently shaken to remove excess microsphere particles. As shown in figure 3.2(a),(c), microspheres initially covered most of the area.

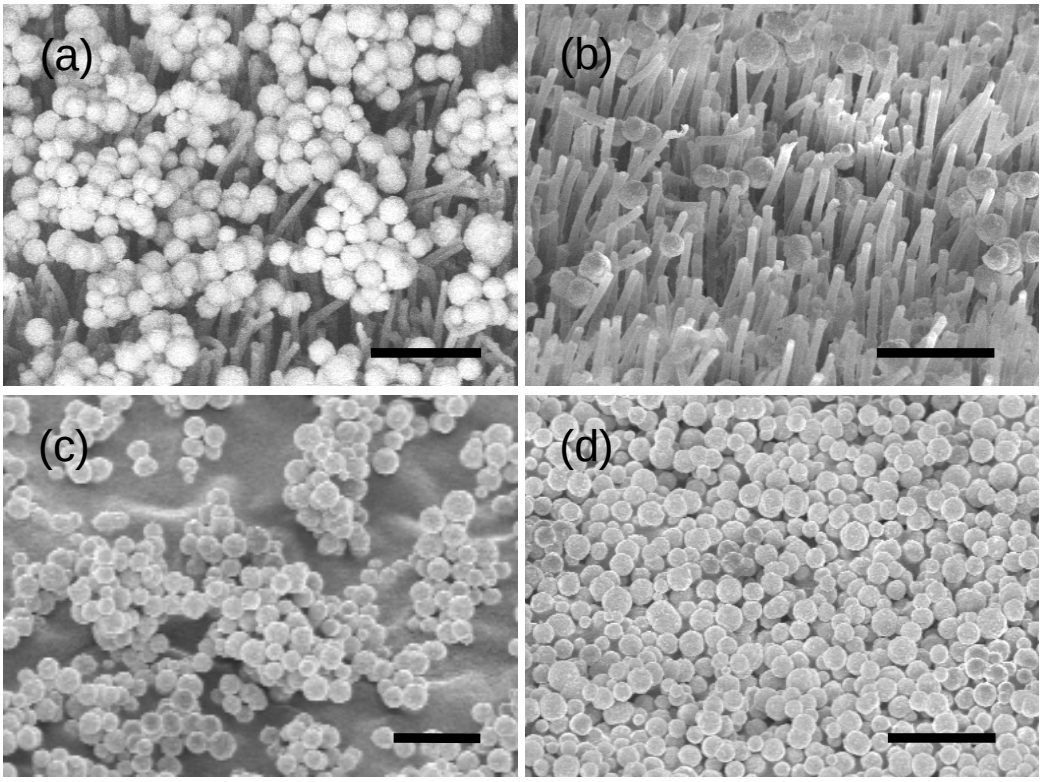

Figure 3.2: Scanning electron micrograph images of the polypropylene fibrillar adhesive and conventional pressure-sensitive adhesives (PSA). (a) Fibrillar adhesive contaminated by gold microspheres. (b) Fibrillar adhesive after 30 contacts (simulated steps) on clean glass substrate. (c) Conventional PSA contaminated by microspheres. (d) Conventional PSA after contacts on a clean glass substrate. All scale bars correspond to 10 μm. Microspheres on fibrillar adhesive are removed by simulated steps, but microspheres on PSA cover more area after the steps.

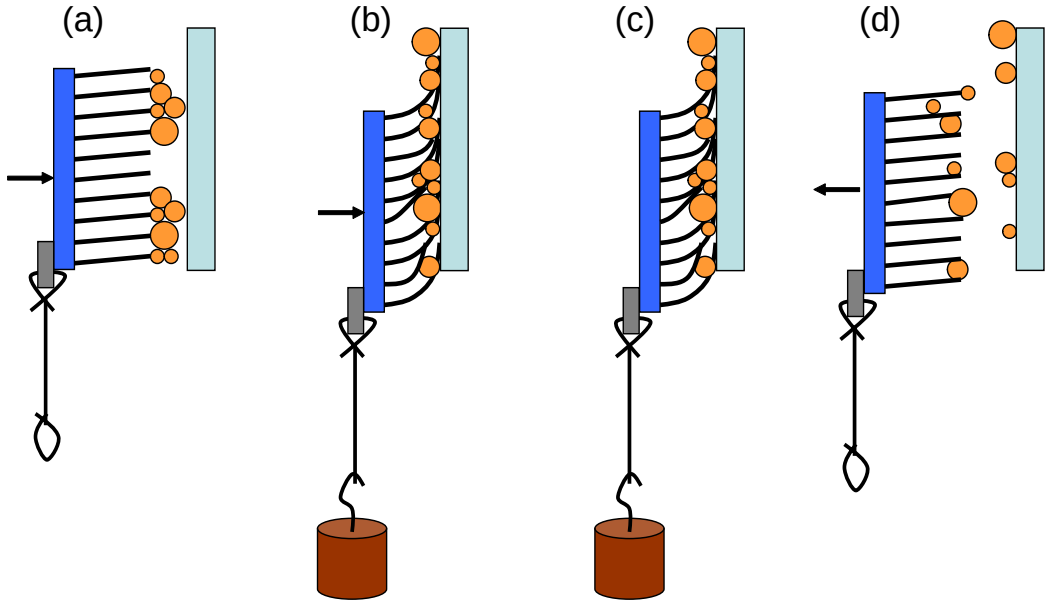

Figure 3.3: One cycle of simulated step, with contact with an initially clean glass slide. (a) Applying normal compressive force. (b) Shear load added to the compressive load by a hanging weight. (c) Removing the compressive load (pure shear loading). (d) Detaching the sample.

3.2.2 Methods

The samples were tested using a simulated step protocol shown in figure 3.3 similar to gecko's walking steps. The samples were first compressively loaded (< 1 N/cm^2) onto a clean glass substrate with a gloved finger (figure 3.3(a)). (It has been shown previously that the shear strength is independent of the initial normal preload [37].) The samples were next loaded parallel to the glass substrate by a weight attached to the load bar through a string (figure 3.3(b)), and then the normal load was removed while maintaining the parallel load (figure 3.3(c)). If the sample could hold the weight, then the sample was removed from the substrate manually (figure 3.3(d)) and increased the weight for the next step. If the sample could not hold the weight, the sample fell and was caught by a gloved hand just below the weight. In case of failure to support the weight, we used the same weight at the next simulated step. Before each "simulated step", the glass substrate was cleaned with isopropyl alcohol to remove residual particles.

3.3 Results and Discussion

3.3.1 Results

After 30 simulated steps, the fibrillar adhesive shed about 60% of the microspheres to the glass substrate as shown in figure 3.2(b). Some microspheres remained embedded between microfibers and were not self-cleaned. As a control, we used a 0.2 cm

$\times$ 0.5 cm conventional pressure-sensitive adhesive (PSA) (Scotch Magic Tape, 3M). After the simulated steps, the soft polymer of the conventional PSA was almost completely covered by microspheres, as shown in figure 3.2(d). This is possibly because microspheres not in direct contact with the soft polymer are taken off and recaptured in the exposed area of the soft polymer during simulated steps.

To quantify the self-cleaning capability of the adhesives, the shear adhesion strength was measured by applying a load parallel to the glass substrate during every simulated step as shown in figure 3.3(c). (The normal compressive load is zero during this phase of the testing cycle; this is not a friction test.) With no contamination, both fibrillar adhesives and PSAs could sustain a 4 N load parallel to a glass substrate (precleaned microscope slides, Fisher Scientific). (We limited the shear force to 4 N to prevent plastic deformation or tearing of the samples' thin backing.) After the samples were contaminated, the initial shear load tried was 0.2 N. This shear load was tested at every simulated step until the sample could sustain it (eight simulated steps for fibrillar adhesive sample 1). Once the sample could sustain this load, the shear load was increased by 0.1 N for the next simulated step. Following 30 successive simulated steps, the fibrillar adhesive sample 1 could sustain a shear load of 1.0 N, but did not show further improvement with five more simulated steps. This saturation is consistent with the quantity of microspheres deposited on the glass substrate after each step, as shown in the bottom three images in figure 3.4. Initial contact steps left many microspheres on the clean glass substrate, with diminishing particle

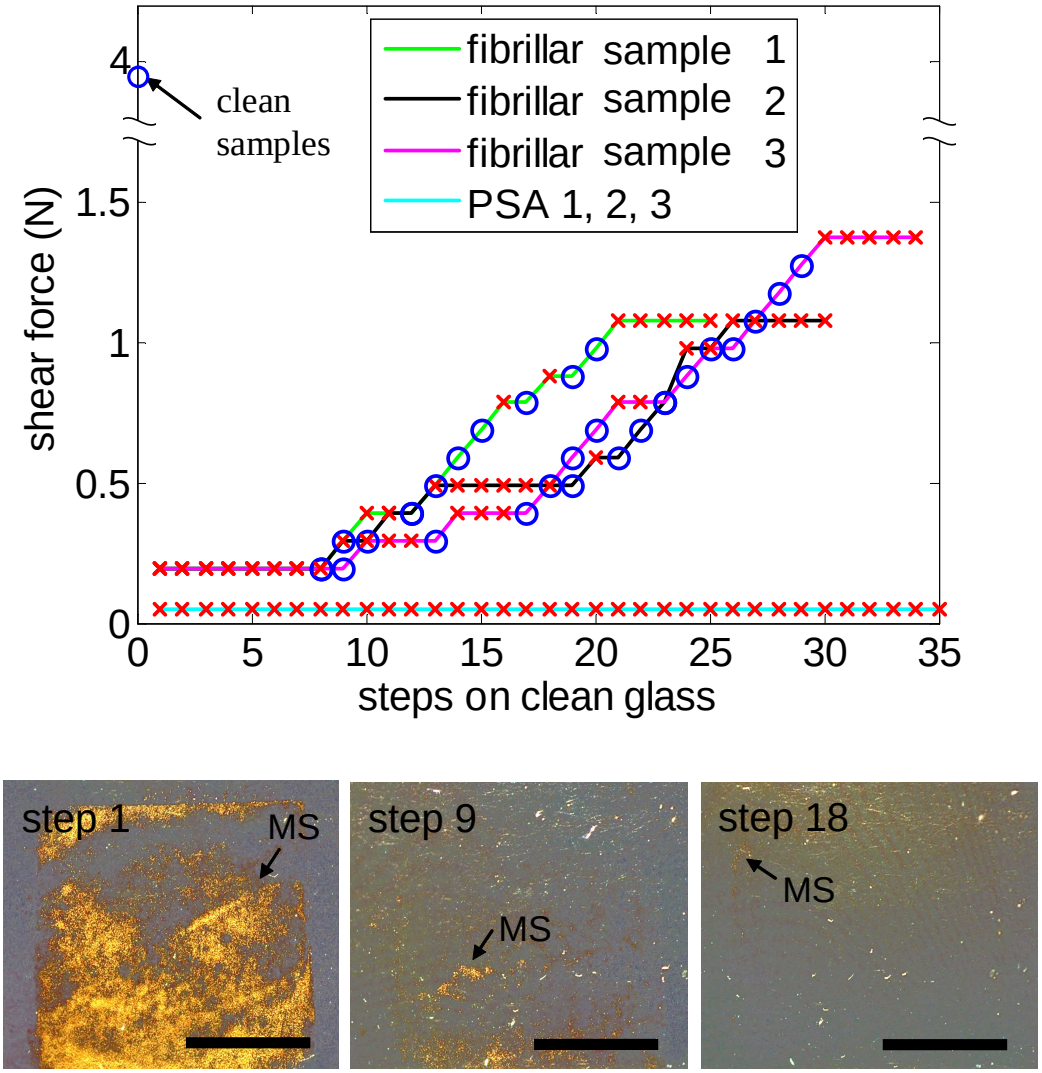

Figure 3.4: Steps on clean glass and recovered shear adhesion. Clean samples could hold 4 N shear force. Samples contaminated by gold particles (mean radius 1.15 μm) recovered up to 33% of the shear adhesion of clean samples. (x) : indicates a shear force that could not be sustained by the adhesive, (o) : indicates the shear force which was sustained. Fibrillar samples 1-3 are separate samples fabricated with same methods. Bottom images: optical images showing the whole contact area after each simulated step (1 cm scale bars). (MS) Microspheres deposited on a glass substrate by fibrillar sample 1 at each step. The quantity of microspheres deposited on the glass decreases with increasing step number.

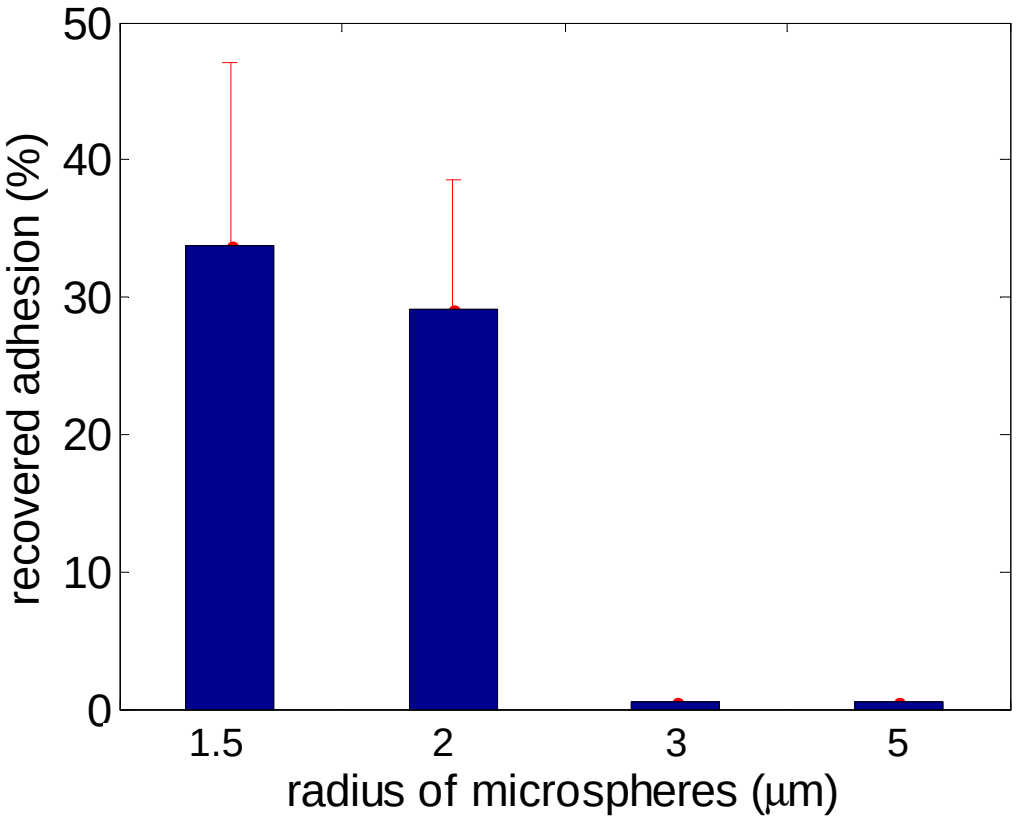

Figure 3.5: Cleaning performance by microsphere size. When the samples were contaminated with 1.5- and 2-μm-radius microspheres, the adhesive force recovered to 33 and 29%, respectively of the clean value after about 20-25 steps. For larger particles (3 and 5 μm), the adhesive force did not recover.

removal after further steps. As expected, the PSA contaminated by microspheres did not recover any shear adhesion and could not sustain 0.05 N, even after 35 steps.

The synthetic fibrillar adhesives did not self-clean larger particles during contact. To observe the self-cleaning dependence on particle size, four differently sized polystyrene microspheres, 1.5 μm, 2 μm, 3 μm (also containing 12% 5 μm) and 5 μm in radius (Corpuscular Inc.), were used as dirt particles. Unlike gold microspheres,

dry polystyrene microspheres contained lumps of microspheres. Because single-sized microspheres are needed, dry polystyrene microspheres were mixed in isopropanol in about a 1:30 ratio. The mixture bottles were ultrasonically agitated (2510 Branson) for 10 min to separate lumps. Then, several drops of the microspheres in isopropanol suspension were deposited on a clean glass slide and air dried. Air-dried polystyrene microspheres became approximately single-layered. The polystyrene microspheres were transferred to fibrillar adhesives by dragging adhesive samples on the glass slide covered with the single-layer microspheres. The shear adhesive strength of clean samples before being contaminated with polystyrene microspheres was 4 N. After testing, fibrillar samples were cleaned by removing clogged microspheres in an isopropanol bath with a table top ultrasonic cleaner (2510 Branson) for 2 min. After ultrasonic cleaning, samples could hold 4 N of shear.

Contaminated samples with uniformly sized polystyrene microspheres were tested with the same methods for gold particles as described in figure 3.4. After about 20-25 simulated steps, samples contaminated with 1.5-μm-radius microspheres recovered about 34% (SD = 13%, three arrays, six measurements) of the shear force of uncontaminated samples, as shown in figure 3.5. Samples contaminated with 2-μm-radius microspheres recovered about 29% of the shear force of uncontaminated samples (SD = 9%, three arrays, six measurements) after 20-25 steps. However, samples contaminated with 3- and 5-μm-radius particles could not sustain 0.2 N in shear (5% of the shear force of uncontaminated samples, three samples, six measurements) even after

25 steps.

3.3.2 Discussion

The contact self-cleaning of the fibrillar adhesives demonstrated above is consistent with a greater affinity of the microspheres for the glass substrate than for the microfibers as described for natural gecko setae [25]. The self-cleaning of natural gecko setae [25] was explained by comparing attraction forces and energies acting on a microsphere in contact with spatulae and a glass substrate. Hansen and Autumn [25] argue that the small number of spatulae contacting a spherical particle have less net adhesive force than particle adhesion to a flat substrate. A similar argument is used here as with Hansen and Autumn [25] for self-cleaning using the Johnson-Kendall-Roberts (JKR) contact model [30] and reported surface energies [62, 44]. Neglecting surface roughness, we can estimate the adhesion forces from the Johnson-Kendall-Roberts (JKR) model [30]. The sphere-glass pull-off force is

$$F_{sg} = \frac{3}{2}\pi R_s W_{sg}$$

and the sphere-fiber pull-off force is

$$F_{sf} = \frac{3}{2}\pi \frac{R_f R_s}{R_f + R_s} W_{sf}$$

with mean radius R_s=1.15 μm for gold microspheres (Alfa Aesar) and microfiber radius R_f=0.3 μm. The work of adhesion is estimated with

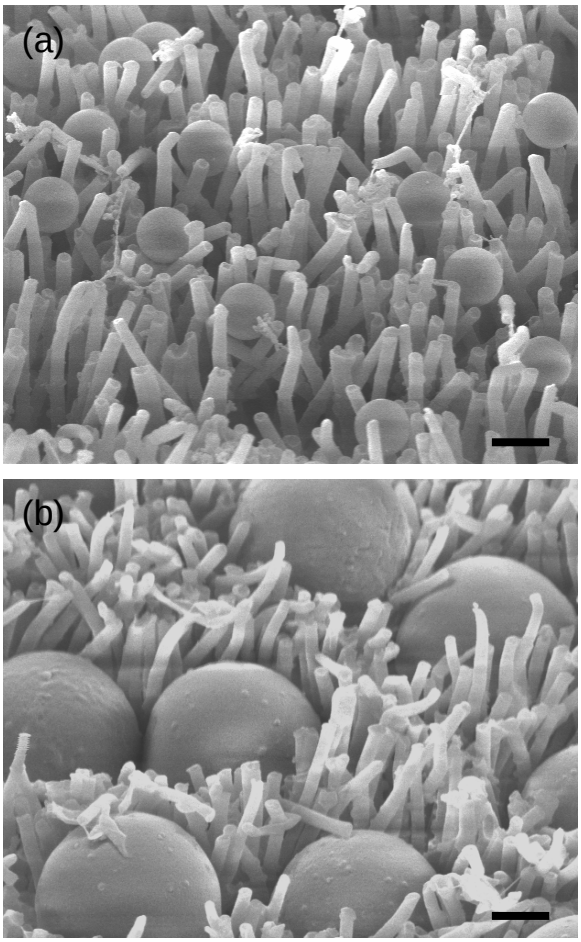

Figure 3.6: SEM images showing two differently sized of microsphere particles on the fibrillar adhesive after simulated steps. (a) The radius of the particles is 1.5 μm. A 1.5 μm particle makes contact with one to four fibers. (b) The radius of the particles is 5 μm. From the density of microfibers and size of a particle, a 5 μm particle makes contact with 33 fibers. From the SEM image, the 5 μm particles are in side contact with fibers. Note that side contact has much more contact area than tip contact. The scale bars are 3 μm.

$$W_{sg} \approx 2\sqrt{\gamma_s \gamma_g}$$

and

$$W_{sf} \approx 2\sqrt{\gamma_s \gamma_f}$$

(ref [28]) where the surface energy is γ_g = 115-200 mJ/m^2 for SiO_2 [62] and γ_f = 30 mJ/m^2 for polypropylene [44]). The ratio of pull-off forces is

$$N = \frac{F_{sg}}{F_{sf}} = (1 + \frac{R_s}{R_f})\sqrt{\frac{\gamma_g}{\gamma_f}}$$

and contact with $N > 9$ microfibers would be required to balance the microsphere-substrate contact. Considering an average microfiber spacing of 1.5 μm, the typical microsphere (mean radius R_s=1.15 μm) will be in contact with one to four microfibers (figure 3.2(b)). Thus, the microspheres are preferentially attracted to the glass substrate instead of the fibrillar adhesive. Note that the ratio of pull-off forces is independent of γ_s. Although we have not tested other substrates, we predict contact self-cleaning for materials with small γ_f compared to γ_g.

Because the sphere-glass pull-off force F_{sg} is proportional to R_s whereas the total sphere-fiber pull-off force $N_f F_{sf}$ is approximately proportional to ${R_s}^2$, (N_f is the number of fibers in the projected area of a microsphere), larger particles will not dry self-clean. The SEM image in figure 3.6 shows that 1.5- (figure 3.6(a)) and 5-μm-radius (figure 3.6(b)) polystyrene microspheres (Corpuscular Inc.) remain in contact

with microfibers after 25 simulated steps. From figure 3.6, a 1.5 μm polystyrene particle is in contact with one to four fibers, whereas 5 μm particles are embedded among fibers, many of which are also in side contact with the microspheres. Note that side contact has much more contact area than tip contact, which makes large particle self-cleaning less likely [40]. From geometry, a 1.5-μm-radius microsphere comes into contact with an average of 3 microfibers whereas a 5-μm-radius microsphere comes into contact with an average of 33 fibers. Hence, it is less energetically favorable to self-clean 5-μm-radius particles than smaller particles. The results of self-cleaning smaller particles and not self-cleaning larger particles support the model that fibrillar adhesives self-clean by unbalanced pull-off forces on smooth surfaces. From the JKR pull-off model, it can be roughly predicted a critical particle size of 5.2 μm radius (with R_f=300 nm, γ_g = 115 mJ/m^2, and γ_f = 30 mJ/m^2). Particles larger than the critical particle size may not be self-cleaned. The overestimation of the predicted critical particle size compared to the 2.5 μm found experimentally (figure 3.5) may be due to uncertainty in the tip shapes of microfibers and possible side contact between microfibers and spherical particles.

The dry contact self-cleaning of one microsphere is illustrated in figure 3.7. Initially, the microsphere is in contact with fibers. When the fibrillar adhesive is preloaded, the microsphere makes contact with the flat glass substrate. During the simulated step, the microsphere may roll [27] or slide [58] as shown in figure 3.7(b), but displacement during a simulated step is quite small compared to the microfiber

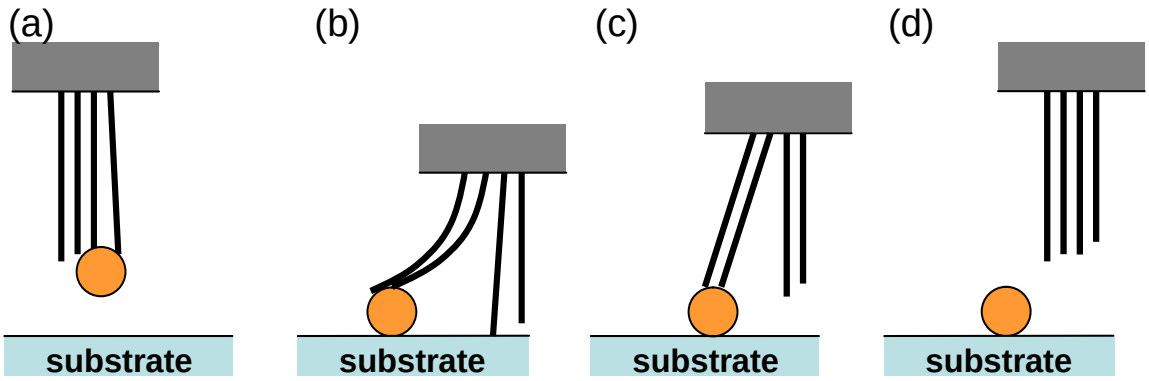

Figure 3.7: Illustration of dry self-cleaning. (a) Before contact. (b) During loading. A microsphere may roll or slide, but it is still in contact with the substrate and fibers. (c) During detachment. A microsphere is under tension between microfibers and substrate. (d) After detachment, with a microsphere deposited on the substrate.

array size, and hence the microsphere maintains contact with the substrate and microfibers before detachment. During detachment, the microsphere is under tension between microfibers and the substrate. At detachment, the microsphere is deposited on the glass substrate as a result of the greater affinity of the microsphere for the glass substrate than for the fibers. Thus, more microfiber tips are exposed to the substrate in the next step, increasing adhesion.

Surface roughness may help self-cleaning [46] by catching particles during sliding, but under our experimental conditions (rms surface roughness of the glass slide scanned with an atomic force microscope (Metrology AFM, Molecular Imaging Inc.) is 3.3 nm), the surface roughness is about 1/1000 of the particle size.

The dry self-cleaning of the natural gecko setae [25] and the synthetic fibrillar adhesive do not use water droplets, which are required for wet self-cleaning (*lotus*

effect) of nonadhesive surfaces. Although only the dry self-cleaning of the fibrillar adhesive is reported in this chapter, the superhydrophobic surface (water contact angle : 150°-160°) of the fibrillar adhesive also shows almost complete wet self-cleaning with water droplets.

3.4 Conclusion

In conclusion, stiff polymer fibrillar adhesives showed self-cleaning properties with microspheres (radius $\leq$ 2.5 μm), as samples recovered 25-33% of the original shear adhesion force after 30 simulated steps. In contrast, shear adhesion in gecko toes recovered 36% of the clean value after only eight steps using a larger particle size (radius $\leq$ 6 μm)[25] even though the contamination method and the simulated step protocol were not exactly the same. The higher efficiency of the natural gecko setae may be from the hierarchical structure of the gecko setae. The natural gecko's spatula tips may push off particles efficiently while switching back and forth between adhesive and nonadhesive states. Also, longer natural setae provide more space between them, thus there may be a higher probability for larger particles to be removed from spatula tips. Experiments with different sized polystyrene microspheres showed that the synthetic fibrillar adhesives did not self-clean larger particles, which is consistent with a JKR pull-off force model. In addition, the large embedded microspheres protrude above the microfiber tips, preventing microfibers from making contacting with the substrate and thus preventing adhesion. It is expected that as fabrication technology

develops further, future hierarchical structured fibrillar adhesives will have thin, flat spatula tips and more space between microfibers and hence will be able to self-clean a wider range of particle sizes with fewer steps as natural gecko setae do.

Chapter 4

Directional Adhesion of Gecko-inspired Angled Microfiber Arrays

Arrays of angled microfibers with a gecko-inspired structure were fabricated from a stiff thermoplastic polymer (polypropylene) with elastic properties similar to those of β-keratin of natural setae. Friction experiments demonstrated that this fibrillar polymer surface exhibits directional adhesion. Sliding of clean and smooth glass surfaces against and along the microfiber direction without applying an external normal force produced an apparent shear stress of 0.1 and 4.5 N/cm^2, respectively. This directional adhesion is interpreted in the context of an elastic bending model of an angled beam. Shearing and normal contact experiments yielded further evidence

of the anisotropic adhesion of the fibrillar polymer and revealed the occurrence of a pull-off (adhesive) force at the instant of surface detachment, unlike vertically aligned microfiber arrays of the same material that exhibited a zero pull-off force. The results of this study provide impetus for the design of gecko-inspired adhesives with angled structures of various hierarchy levels that demonstrate directional adhesion against different material surfaces.

4.1 Introduction

Angled natural gecko setal arrays consisting of β-keratin (elastic modulus E = 1.5 GPa) [45, 11] are characterized by a high normal compliance [11] that is a key factor in producing high adhesion and directional properties, such as pure adhesion and high friction when sliding occurs along and against the setal direction, respectively [6]. The unique directional properties of these hard-material-based angled setal arrays provide controllable [6, 24] and self-cleaning [25] adhesion, enabling geckos to run up vertical walls as fast as 1 m/s [24].

Angled microfibers are of critical importance in the design of gecko-like surfaces with adjustable adhesion properties [59]. Significant effort has been devoted to fabricate angled stalk arrays showing adhesion behaviors similar to those of gecko setae. For example, Santos et al. [53] designed angled point-stalks of polyurethane (E $\approx$ 0.3 MPa), Aksak et al. [1] and Murphy et al. [41] fabricated angled fiber arrays with and without spatula tips consisting of two different types of polyurethane (E $\approx$ 2.9 and

9.8 MPa), and Yao et al. [61] examined the properties of a thin-film layer deposited on tilted stalks of polydimethylsiloxane (E $\approx$ 3 MPa). These structures demonstrate directional properties characteristic of gecko-inspired synthetic adhesives [7]. However, angled fibrillar adhesives consisting of a hard polymer that exhibit anisotropic properties have not been fabricated yet.

Since hard and smooth polymers do not generate significant adhesion even down to the millimeter scale, they are promising materials for gecko-inspired synthetic adhesives demonstrating high durability and self-cleaning capability [25, 36]. Therefore, the main objective of this study was to investigate whether gecko-inspired adhesives consisting of angled microfiber arrays can be fabricated from a hard polymer with mechanical properties similar to those of β-keratin of natural setae, such as polypropylene.

4.2 Materials and Methods

4.2.1 Materials

Vertically aligned arrays of high-density microfibers were fabricated by casting a 25-μm-thick layer of polypropylene (TF-225-4, Premier Lab Supply) in vacuum at 200°C into a 20-μm-thick polycarbonate track etched membrane filter (ISOPORE, Millipore) with 42×10^6 pores/cm^2 of 0.6 μm pore diameter, as described in figure 4.1(a,b). Tensile tests (Sintech tensile tester 2/S, MTS Systems) revealed a polypropy-

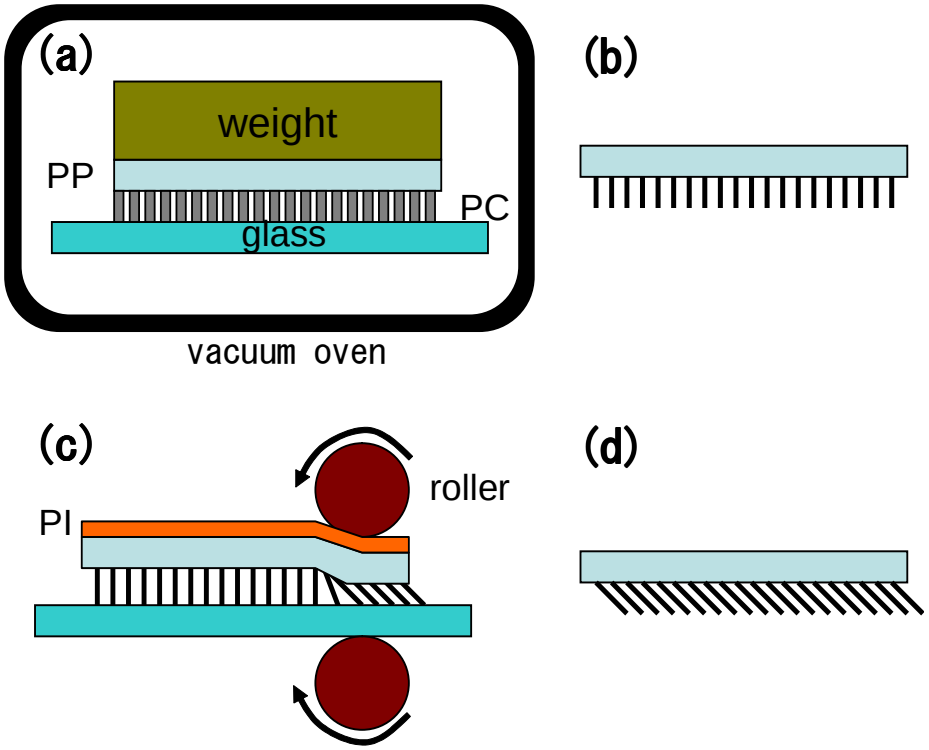

Figure 4.1: Schematic illustration of the fabrication process of angled microfiber arrays (a) Polypropylene (PP) is melted into a polycarbonate(PC) template in vacuum oven at 200°C for 28 minutes. (b) The polycarbonate template is etched in methylene chloride and the sample is rinsed in isopropanol. (c) A vertically aligned microfiber array is passed between rollers heated at 50°C, while a polyimide (PI) film prevents sample adhesion to the hot rollers. (d) Resulting angled microfiber array.

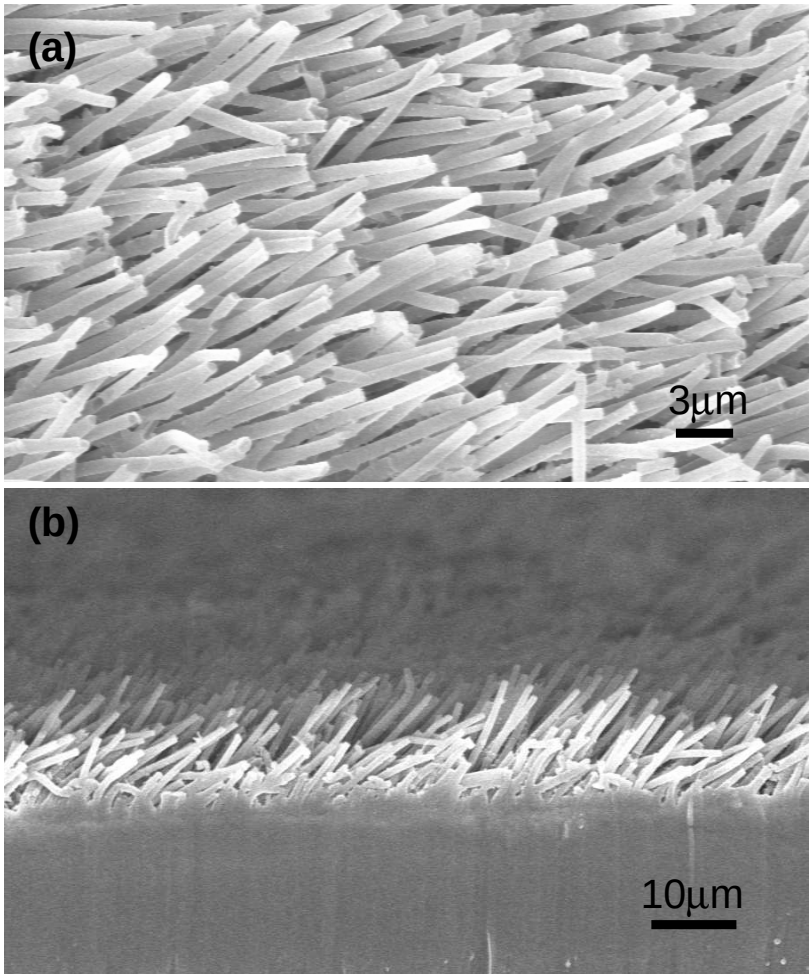

Figure 4.2: SEM images of the produced fibrillar adhesive. (a) Top view of angled fibrillar adhesive. (b) Side view of angled fibrillar adhesive. Average angle of microfibers from vertical axis is 45°.

lene elastic modulus of ~ 1.5 GPa. The vertically aligned microfiber array patch was covered by a 25-μm-thick polyimide film placed on a clean microscope glass slide (Fisher Scientific), and the stack was processed by rollers (Catena 35, General Binding Corporation) that were heated at 50°C [figure 4.1(c)] to form angled microfiber arrays [figure 4.1(d)]. Scanning electron microscope (SEM) images of top and side views of fabricated angled microfiber arrays are shown in figures 4.2(a) and 4.2(b), respectively. The average tilt angle of the unloaded microfibers from the surface normal is $\theta_0 = 45°$ and the average center-to-center microfiber distance is equal to 1.5 μm. The size of the microfiber arrays used in the one- and two-axis force measurements described below was 2×2 cm^2 and 2×5 mm^2, respectively.

4.2.2 Methods

The directional adhesion behavior of the 2×2 cm^2 samples was examined with a custom-made one-axis force sensor [37] that measures the shear force F_s due to sliding a microfiber array against a substrate without applying a normal force F_n (see more details on the force sensor in appendix.) Before each test, the angled microfiber array was placed on a glass substrate cleaned with isopropanol and a normal force was applied to generate an apparent compressive stress of 0.1 N/cm^2. Then, the normal force was removed and the entire stage, including the glass substrate, was displaced laterally either along or against the microfiber direction at a constant speed of 120 m/s. Although testing was performed under a zero external normal force, a very

small compressive stress of 0.5 mN/cm^2 due to the sample weight was applied to the microfibers. The estimated microfiber contact area was determined from in situ observations obtained with a camera, using frustrated total internal reflection at the interface of the side-illuminated glass substrate and the microfiber array [37, 14]. It is assumed that all microfibers in the estimated microfiber contact area are in contact with the glass substrate.

In addition to the tests with the one-axis force sensor, experiments were also performed with a two-axis force sensor to further examine the directional adhesion of the fibrillar adhesive and the development of a pull-off (adhesive) force at the instant of surface separation after pure normal loading. Instead of a spherical indenter used in earlier studies [55], the sample was attached to a flat glass indenter (figure 4.3) by cyanoacrylate instant adhesive (495, Loctite) and aligned co-planar with a clean glass substrate using a high-magnification lens (Edmund Scientific) and a viewing camera (MicroPublisher 5.0 RTV, QImaging). In all of the sliding tests with the two-axis force transducer the sliding speed was fixed at 10 m/s.

4.3 Results and Discussion

The evolution of the shear force due to sliding along and against the microfiber direction in the absence of an external normal force is shown in figure 4.4. The plot contains two types of results: (a) statistical results, i.e., mean (solid curve) and standard deviation (error bars) shear force data obtained from seven tests in which

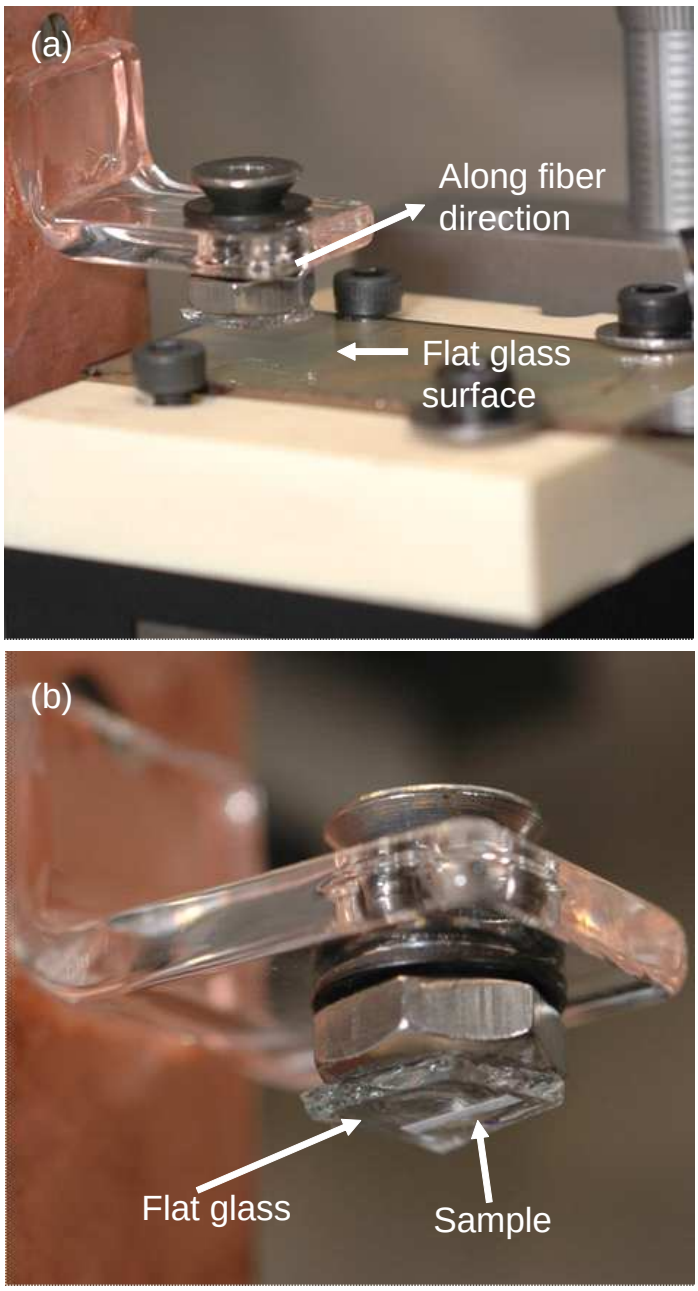

Figure 4.3: Flat indenter

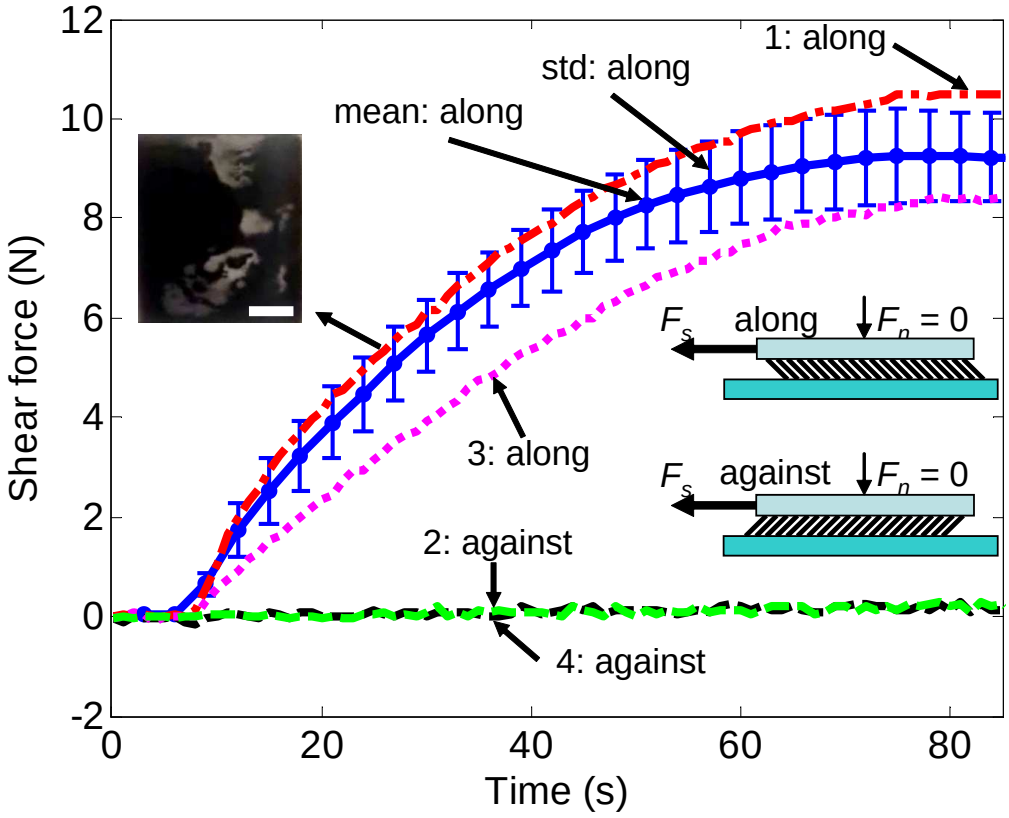

Figure 4.4: Evolution of shear force of angled fibrillar adhesive during sliding in the absence of an external normal force. Average (solid line) and standard deviation (error bars) data were obtained from seven tests in which sliding occurred along the microfiber direction. The testing sequence in the multiple-sliding experiment was along (dash-dot line 1), against (dash line 2), along (dot line 3) and, finally, against (dash line 4) the microfiber direction. The inset shows an optical image of contact regions (bright spots) used to estimate the microfiber contact area for sliding along the microfiber direction (scale bar = 5 mm).

sliding occurred along the microfiber direction and (b) typical shear force responses due to sequential sliding along and against the microfiber direction (discontinuous curves 1-4). Sliding along the microfiber direction enhanced the sample engagement, leading to an increase in the shear force (curve 1). This trend is attributed to the continuously increased contribution of adhesion to the shear force needed to maintain sliding, caused by the increase of the real contact area with the surface conformity as a result of microfiber bending. Although subsequent sliding against the microfiber direction produced a very small shear force (curve 2), sliding again along the microfiber direction yielded an increase in shear force (curve 3) similar to that observed initially (curve 1). Finally, sliding against the microfiber direction yielded again a shear force close to zero (curve 4), illustrating repeatable directional adhesion.

The mean shear force due to sliding along the microfiber direction [solid curve, figure 4.4] consists of three regimes. The zero shear force up to ~ 8 s from the onset of sliding (first regime) is due to the slack string connected to the force sensor that inhibited microfiber slip. The subsequent increase of the shear force (second regime) represents a transient period in which continuous bending of contacting microfibers resulted in more microfiber contact that increased the real contact area and, in turn, the shear force to maintain sliding. Equilibrium was reached at the microfiber/glass interface after sliding for ~ 60 s along the microfiber direction, resulting in a steady-state shear force of $8-10$ N (third regime).

The directional dependence of the shear force [figure 4.4] can be interpreted in the

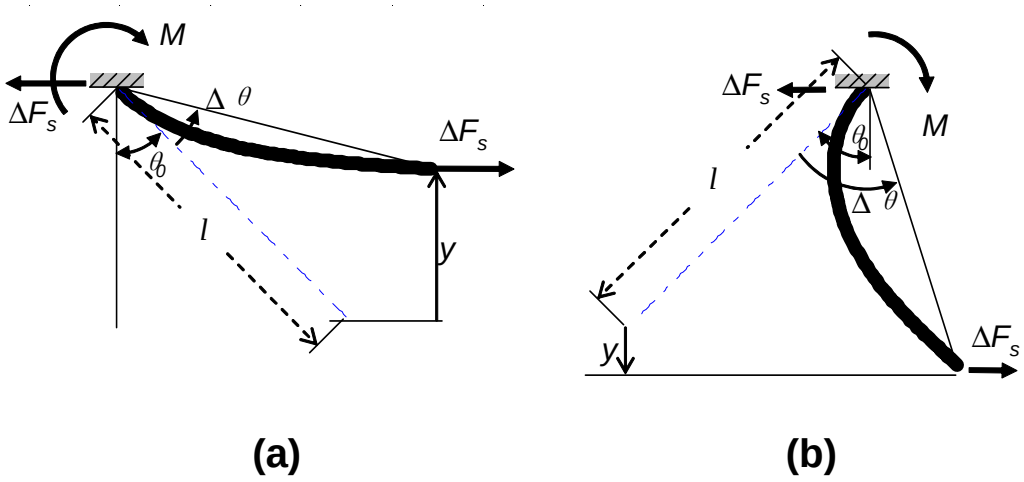

Figure 4.5: Schematics of an angled microfiber undergoing bending due to sliding (a) along and (b) against the microfiber direction in the absence of an external normal force.

context of an elastic bending model of an angled beam. Previous analyses provided insight into the dependence of the contact force at a fiber tip on the fiber angle and sliding direction [59], and the variation of the normal force at a flat tip with the fiber angle and deflection [1]. Since the normal pressure due to the sample weight can be ignored as negligibly small, the angle $\theta(s)$ from the surface normal due to a shear force applied at the free end of a microfiber $\triangle F_s$ [figure 4.5], where s is the distance from the fixed end of the beam, is the solution of the following differential equation derived from elastic beam theory.

$$EI\frac{d^2\theta}{ds^2} + \triangle F_s \cos\theta = 0 \tag{4.1}$$

where I $(= \pi r^4/4)$ is the moment of inertia, r is the microfiber radius, $\theta(= \theta_0 + \triangle\theta)$is the angle from the surface normal, and $\triangle\theta$ is the deviation angle from θ_0 due

to the shear force $\triangle F_s$.

The microfiber density n of the fibrillar adhesive [figure 4.2] is equal to the filter pore density (42×10^6 pores/cm^2). For steady-state sliding along the microfiber direction (i.e., $F_s \approx 9$ N), the estimated microfiber contact area A, determined from seven tests (Image processing toolbox, Matlab, Mathworks), was found equal to 0.18 ($\pm$0.02) times the apparent contact area (4 cm^2). Hence, the steady-state shear force per microfiber ($\triangle F_s = F_s/nA$) due to sliding along the microfiber direction [figure 4.5(a)] is estimated to be $\triangle F_s \approx 298$ nN. For $l = 18$ μm, $r = 0.3$ μm, $E = 1.5$ GPa, and $\triangle F_s = 298$ nN and boundary conditions $\theta(0) = 45^\circ$ and $M(l) = 0$, numerical integration of Eq. 4.1 (Matlab, Mathworks) yields $\triangle\theta = 31^\circ$ [figure 4.5(a)]. Thus, the increase of the shear force to a steady-state of ~ 9 N [solid curve, figure 4.4] is attributed to the increase of the real contact area due to microfiber bending that increased the number of microfibers in contact with the substrate and, in turn, the contribution of adhesion to the total shear force. For sliding against the microfiber direction, $F_s \approx 0.2$ N [e.g., curves 2 and 4 in figure 4.4] and A is ~ 0.01 times the apparent area (observed in situ as described earlier). Thus, the estimated steady-state shear force is $F_s \approx 119$ nN. For boundary conditions $\theta(0) = -45^\circ$ and $M(l) = 0$, numerical integration of Eq. 4.1 yields $\triangle\theta = 71^\circ$. Thus, sliding along the microfiber direction produced a much higher shear force (by a factor of 2.5) and less bending than sliding against the microfiber direction. From the numerical solution, the backing-substrate distance was predicted to decrease by y = 8.4 μm [figure 4.5(a)].

Since this gap decrease is much larger than the microfiber height variation ($\sim$ 3 m), a significant increase in the number of contacting microfibers (or real contact area) is predicted for sliding along the microfiber direction. Alternatively, an increase in the backing-substrate gap by y = 2.5 μm [figure 4.5(b)] was calculated for sliding against the microfiber direction, suggesting that even microfibers initially in contact with the glass substrate were detached during sliding, resulting in a significant decrease in the real contact area and, in turn, negligibly small shear force. These arguments are in agreement with experimental measurements of the estimated microfiber contact for sliding along (0.72 cm^2) and against (0.04 cm^2) the microfiber direction.

Figures 4.6 and 4.7 show shear and normal force responses of angled and vertical microfiber arrays obtained from sliding (under a fixed normal displacement) and pure normal contact experiments performed with a displacement-controlled two-axis stage. As shown in figure 4.6(a) and 4.6(c), sliding along the microfiber direction, while maintaining the normal displacement that produced a normal force (preload) F_n = 0.5 and 1.0 mN, respectively, resulted in pure shear loading throughout most of the test duration. The negative shear force during preloading is attributed to the force applied to the flat indenter by the compressed microfibers. Surface separation at the end of sliding produced a small tensile (negative) normal force. A markedly different behavior was observed when sliding occurred against the microfiber direction under identical preloads. As evidenced from figure 4.6(b) and 4.7(d), a marked increase in the shear force and a high normal force were produced in this case, resulting in a

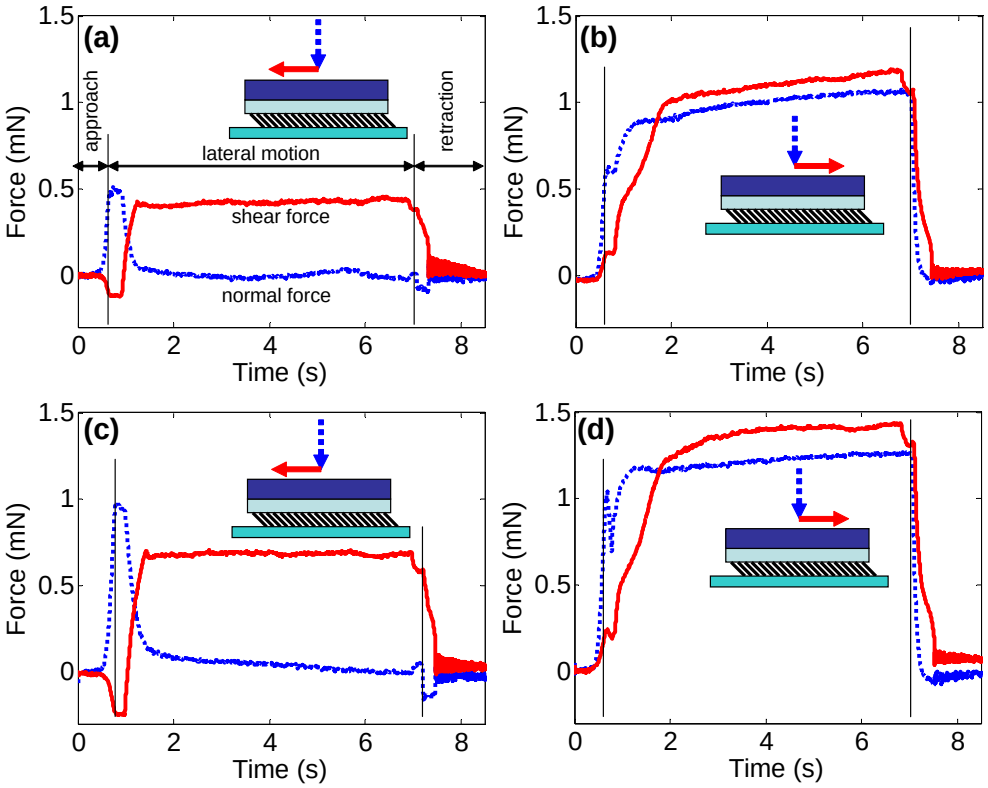

Figure 4.6: Shear force responses of angled microfiber arrays for sliding (a,c) along and (b,d) against the microfiber direction under a fixed normal displacement produced by applying a normal force (preload) of 0.5 and 1 mN

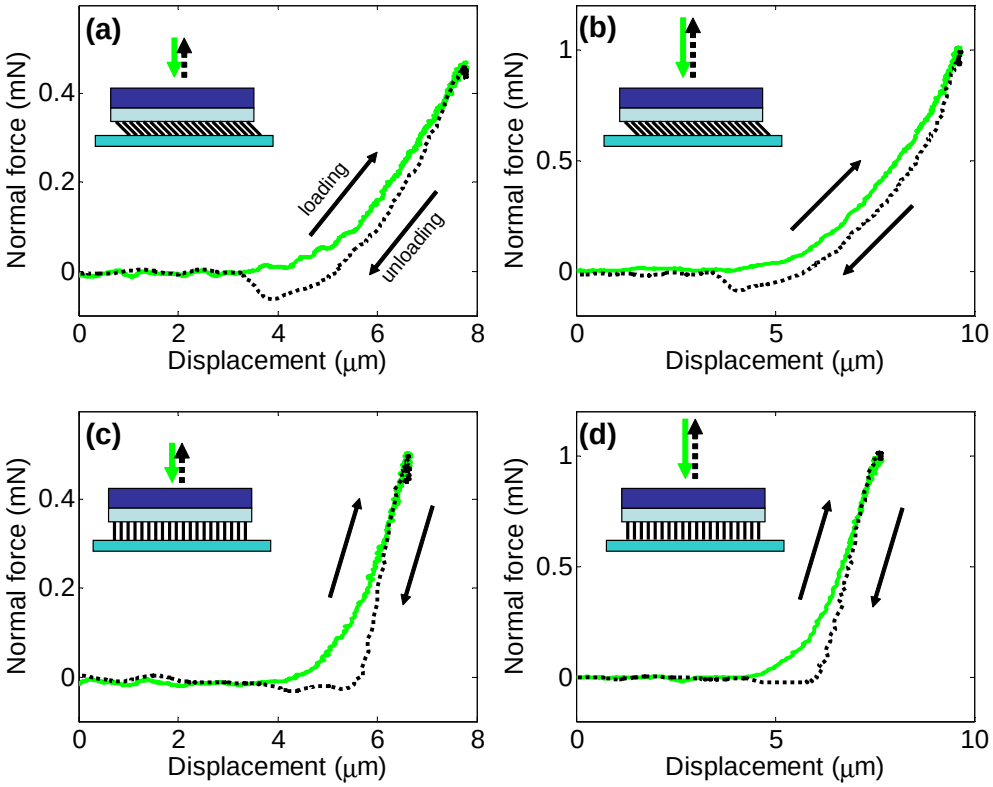

Figure 4.7: Normal force vs displacement responses of (a,b) angled and (c,d) vertically aligned microfiber arrays.

high coefficient of friction of 1.1. Furthermore, a negative (tensile) normal force was not observed at the instant of surface separation. Therefore, even at the millimeter scale, the angled microfiber array demonstrated pure adhesion in one direction and high sliding friction in the opposite direction. Furthermore, the existence of a force hysteresis in all of the normal contact responses [figure 4.7] suggests that energy dissipation occurred at the contact interface as a result of microfiber slip. In addition, a tensile (adhesive) pull-off force was measured at the instant of surface separation of the angled microfiber array [figure 4.7(a) and 4.7(b)], as opposed to the vertically aligned microfiber array that produced a virtually zero pull-off force [figure 4.7(c) and 4.7(d)].

4.4 Conclusion

In conclusion, gecko-inspired angled fibrillar adhesives fabricated from a hard polymer (polypropylene) demonstrated pure adhesion in one direction and high sliding friction in the opposite direction, similar to gecko setal arrays. The anisotropic adhesion of the angled microfiber arrays was interpreted in the context of an elastic bending model of an angled beam. A significant pull-off force was observed at the instant of surface separation of the angled microfiber array after pure normal contact, indicative of its higher compliance (hence, higher adhesion) compared to arrays of vertically aligned microfibers. Future versions of this gecko-inspired fibrillar adhesive are envisioned to be arrays of angled microstructures exhibiting various hierarchy lev-

els, including thin flat spatulae and lamellae that would provide directional adhesion even on rough surfaces. Angled fibrillar adhesives can be used in a wide range of applications, such as one-directional clutches, temporary adhesives, sport goods for climbing, and automotive tires.

Chapter 5

Conclusion

This work describes development of a biologically inspired synthetic fibrillar adhesive from hard polymer microfiber arrays.

5.1 Contribution

Hard polymer is basically non-tacky. Because its high stiffness, smooth clean polymer does not have noticeable adhesion in macro scale even on clean smooth glass. Thus, synthetic adhesive from hard material is more controllable and can avoid adhesion with unwanted surfaces or particles as with natural gecko setae.

5.1.1 Sliding enhanced shear adhesion

Shear adhesion is achieved with hard polymer microfiber arrays. In addition to static adhesion, shear force increases when the vertically aligned microfiber arrays

slides on a smooth glass substrate. The adhesive is durable for more than 100 uses over 6 months.

5.1.2 Self-cleaning synthetic fibrillar adhesive

Self-cleaning of the synthetic microfiber adhesive from hard polymer is investigated. Contaminated fibrillar adhesive with the dirt particles recovers adhesion as repetitively used on the smooth dry glass substrate.

5.1.3 Directional adhesive from angled microfiber arrays

Angled microfiber arrays are fabricated and used to demonstrate directional adhesion. Without compressive normal load, the angled microfiber array develops adhesion when dragged along the microfiber direction and does not when dragged against the microfiber direction.

5.2 Application

Conventional tapes are widely used including office products, medical and construction materials etc. Most of these tapes are for one time use due to soft polymers which are easy to degrade and collect dirt particles. The stiff polymer (that is more durable) based synthetic gecko adhesives have potential for diverse applications such as medical material, climbing robots, sporting goods, apparel and car tires etc.

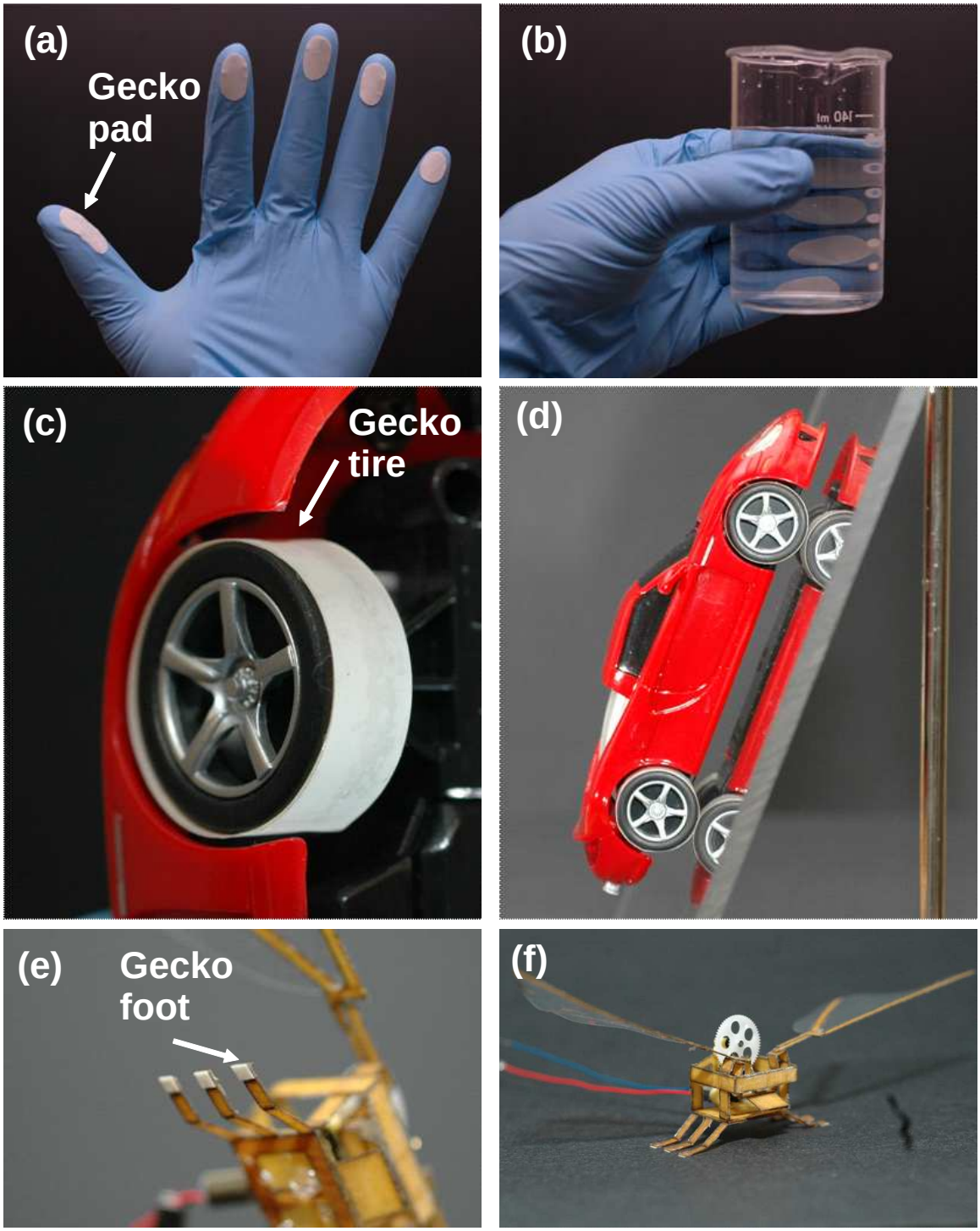

Figure 5.1: Applications for synthetic gecko adhesive. (a) and (b) gecko gloves for better griping with low normal pressure. (c) and (d) gecko tires for better braking and traction. (e) and (f) gecko feet for a flying robot for landing on vertical or inverted surfaces. The flying robot was designed and built by Stanley Baek in UC Berkeley.

For example, as shown in figure 5.1(a) and (b), gecko adhesive can be used in gloves or robot fingers for better griping especially when holding fragile objects with low normal pressure. Another potential application is car tires as shown in figure 5.1(c) and (d) for better braking and traction. In order to be used in car tires, durability under harsh condition should be improved. In its early stage, gecko tires can be used for racing for limited time. Easily detachable gecko tapes also can be used in climbing and flying robots which can go dangerous places as shown in figure 5.1(e) and (f). Climbing robots can be used as a window cleaning robot on high rising buildings, and flying robots able to land on a ceiling can be used as a surveillance robot. In addition, synthetic gecko tape can be used as medical tapes. For example, synthetic gecko tapes fixing tubes on a human skin can be detached without pain to patients.

5.3 Future Works

The developed fibrillar adhesives are working well in the controlled environments, i.e., clean smooth surfaces. The adhesives have high shear adhesion but low normal adhesion with the self-cleaning property. My future goal is to make robust hard material based fibrillar adhesive working in general environments, i.e., rough surfaces. Custom made templates (one example in figure 5.2) are required to make more complex structures or to change diameter, length, and density of microfibers for mechanically controllable adhesion on various surfaces. To develop versatile fibrillar adhesive

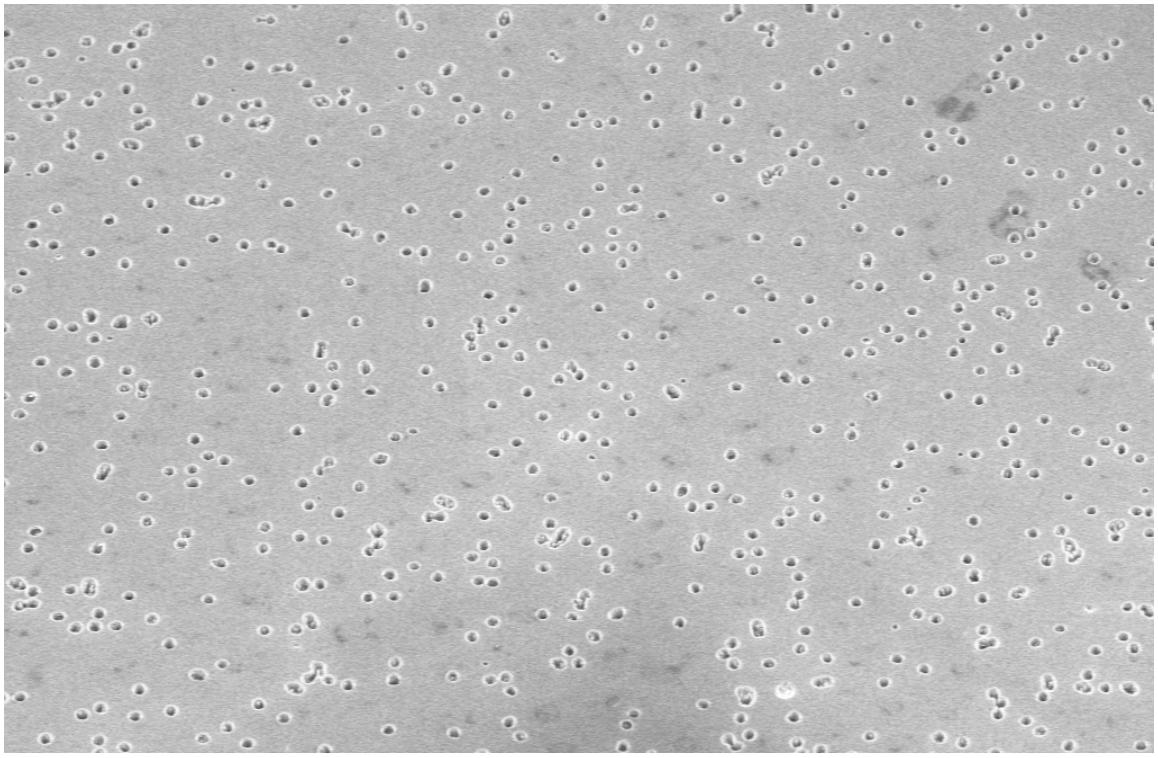

Figure 5.2: A custom made template to control length, diameter and density of microfibers.

similar to natural gecko adhesive, the following two factors should be addressed.

5.3.1 Enhanced adhesion with thin flat spatula tips

Surface fibrillation, intended to give compliance, significantly reduces cross-sectional area. Uniform circular rods can have side-contact with a substrate when shear force is applied. However, when shear force is removed, the elastic uniform rods tend to recover their original shape, resulting in small normal adhesion. If the tips are tailored to thin and flat, the recovering elastic energy may balance with adhesive force of flat spatulas, resulting more robust adhesion.

5.3.2 Branched fibrillar adhesive for rough surfaces

To adhere to rough surfaces with fiber arrays, relative long fibers are required to conform to the rough surface. However, too long slender fiber arrays may result in clumping each other and too short or thick fiber arrays cannot conform to rough surfaces and lower adhesion even on smooth surfaces. One solution for rough surface could be branched fibers. Main fibers could be long and thick to prevent the fibers from clumping, and branched slender fibers at the tips could help conforming to and increasing adhesion on rough surfaces.

Appendix A

Adhesive force measurement apparatus

It is important to find out and characterize properties of synthetic gecko adhesive after designing and fabricating. Force sensor apparatuses were designed and built up to measure static and sliding adhesive forces in centimeter scale synthetic adhesive samples. Also, using optical method, microfiber contact area was quantified to explain static and sliding adhesive forces.

A.1 Static force measurement apparatus

The static force measurement apparatus was built for shear, normal and peel tests as shown in figure A.1. Replaceable substrate surface can be tilted to measure pure shear adhesive force (figure A.1(a) and (b)) and normal adhesive force (figure

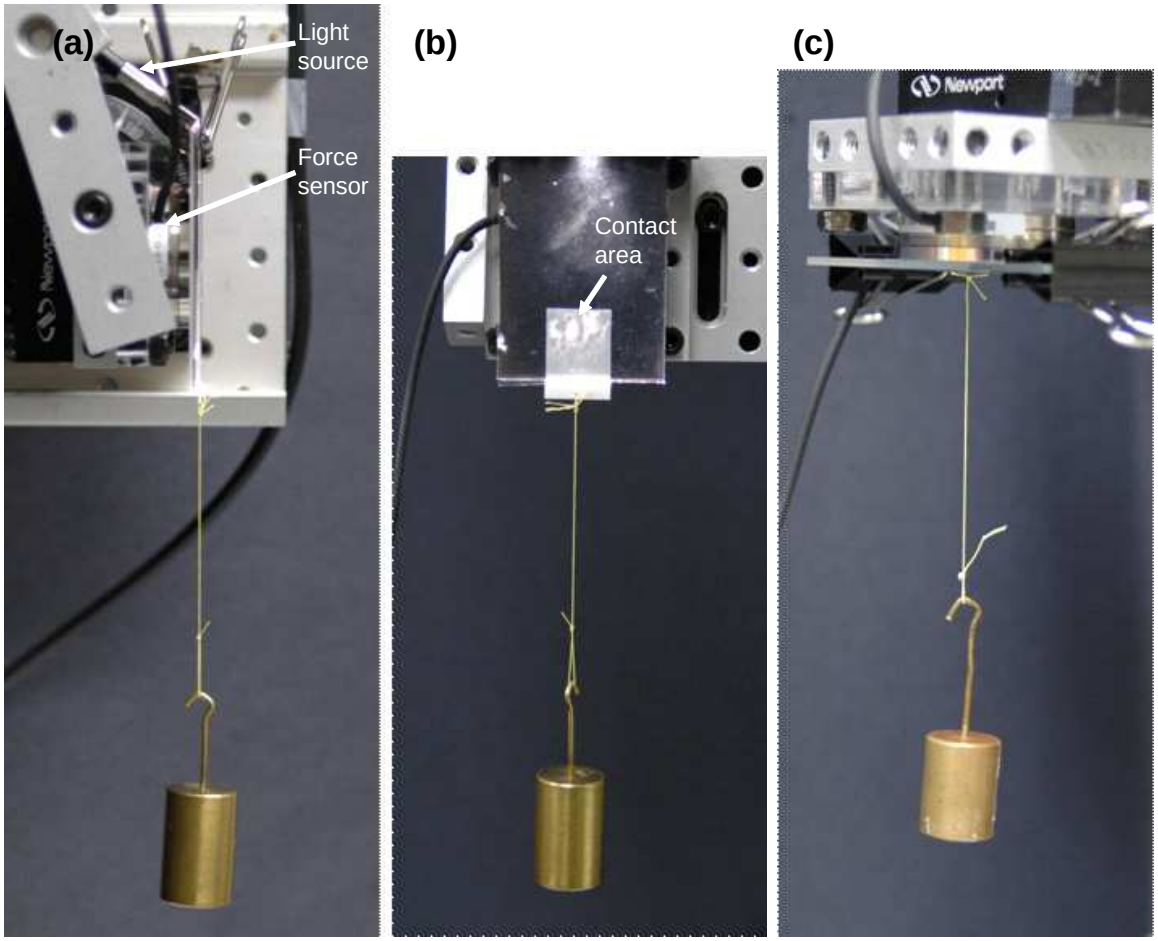

Figure A.1: Static adhesive force measurement apparatus. (a),(b) Side and front view of shear force measurement respectively. The light source is used to illuminate contact area (bright spots in (b)) and the force/torque transducer is used to monitor preload. (c) Normal force measurement by tilting the substrate.

A.1(c)). To measure peeling angle, the substrate surface can be tilted from vertical to horizontal with a weight hanging. A 6-axis force and torque transducer (Nano43, ATI Industrial Automation) fixed under the glass substrate is used to monitor shear and normal forces as well as preload. The light source as in figure A.1(a) was applied through the glass substrate to illuminate microfiber contact area (bright spots) in A.1(b). The contact area monitoring apparatus accelerated the research by helping to explain measured forces and providing intuition on ways to increase contact area.

A.2 Sliding force measurement apparatus

From manual tests, the synthetic gecko adhesives kept adhesion even while sliding. To systematically measure and quantify sliding behaviors of natural and synthetic gecko adhesive, the sliding force measurement apparatus was designed and built up as shown in figure A.2. A sample is placed on the linear motor driven stage. The sample is connected to the custom made double cantilever and deflection of the double cantilever is measured by the optical sensor. Sliding distance is measured by the linear variable differential transformer (LVDT, MEPTS-9000, Techkor Instrumentation). Microfiber contact area is illuminated by the light source and and the light source is blocked by the shade for better contrast. The contact area is monitored and recorded by a camcorder. The video files are captured and processed to quantify contact area while samples are sliding.

Three double cantilevers were made for different ranges of shear force depending

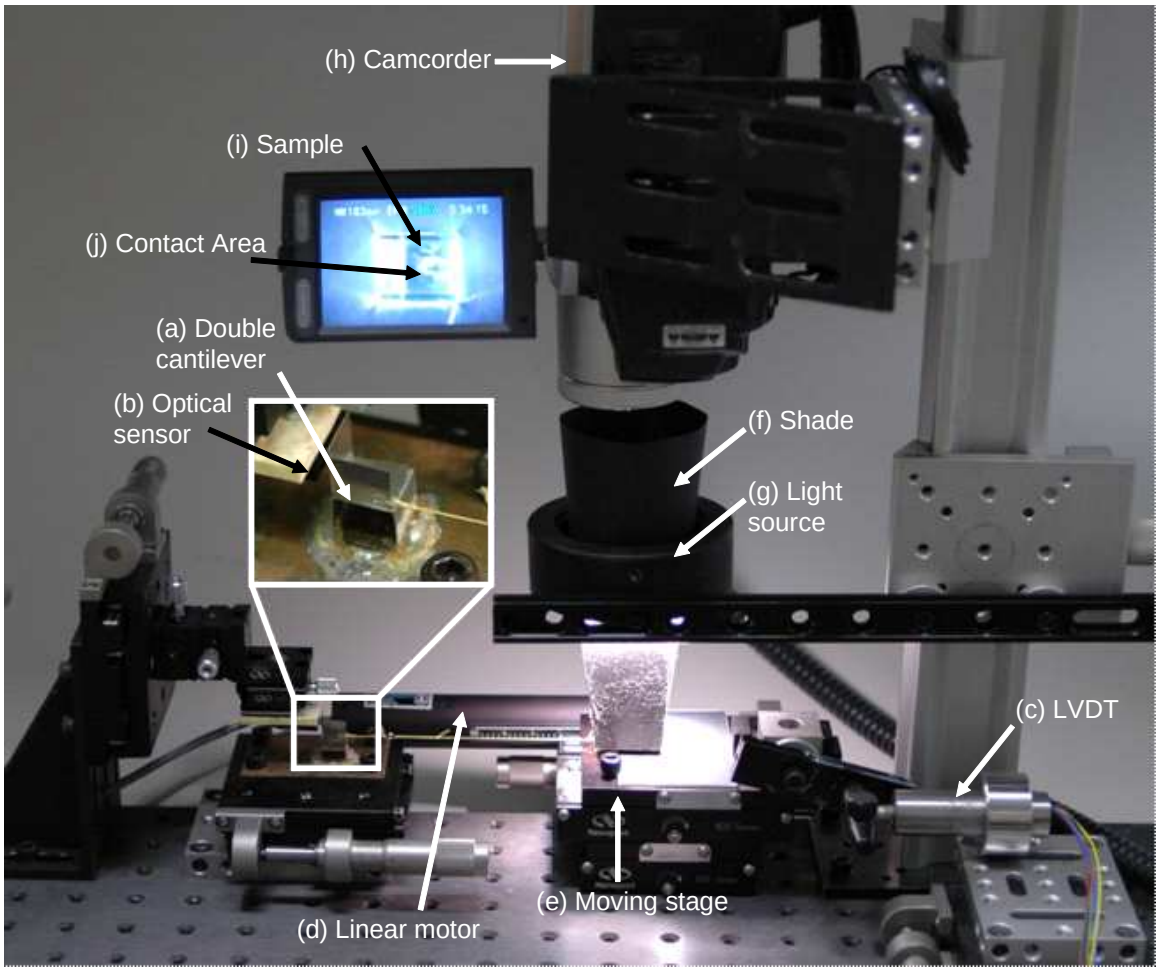

Figure A.2: Sliding force measurement apparatus.

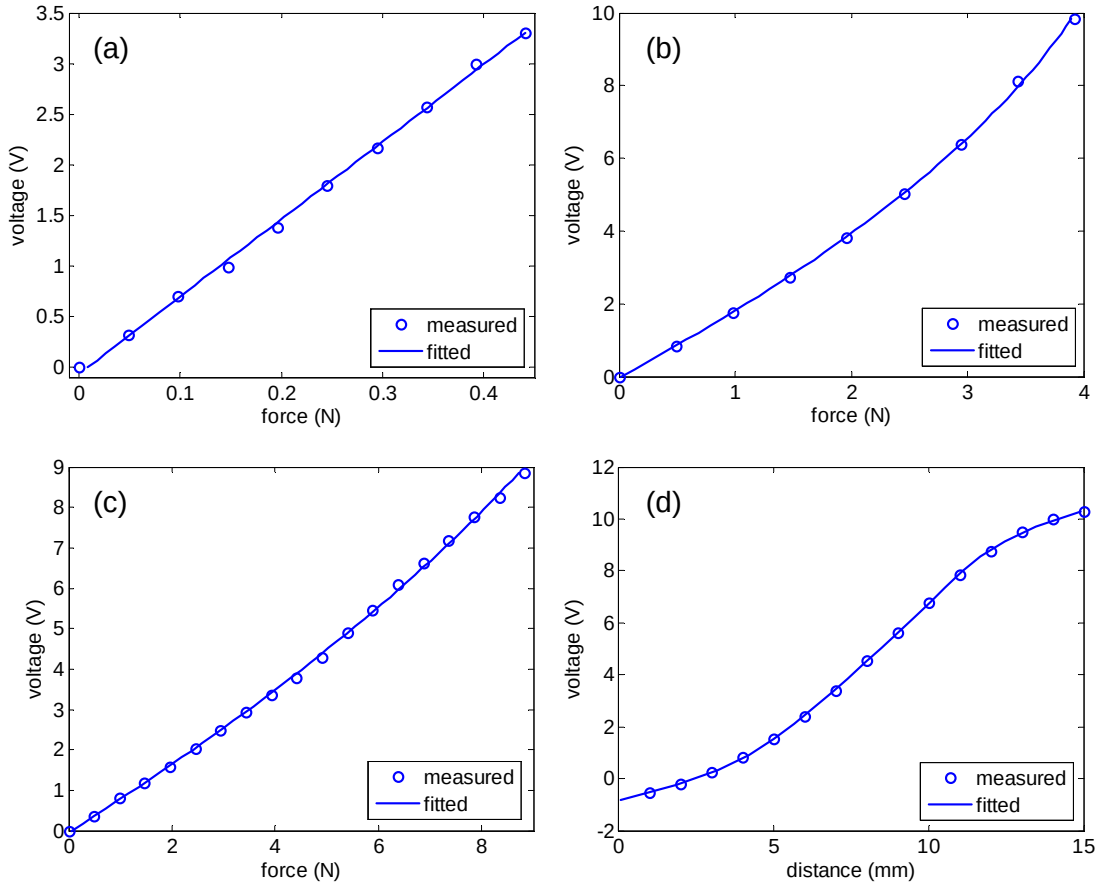

Figure A.3: Calibration charts for three force sensors ((a),(b),(c)) and for (d) LVDT.

on types of samples. Each double cantilever was calibrated with known weights as shown in figure A.3(a), (b) and (c). The calibration chart (a), (b) and (c) in figure A.3 were used for small size of natural gecko lamellae, vertically aligned synthetic microfiber arrays and synthetic angled microfiber arrays respectively. LVDT was also calibrated with a micrometer and the chart is shown in figure A.3(d).

Bibliography

[1] B. Aksak, M. P. Murphy, and M. Sitti. Adhesion of biologically inspired vertical and angled polymer microfiber arrays. *Langmuir*, 23:3322–3332, 2007.

[2] B. Aksak, M. Sitti, A. Casell, J. Li, M. Meyyappan, and P. Callen. Friction of partially embedded vertically aligned carbon nanofibers inside elastomers. *Applied Physics Letters*, 91:061906, 2007.

[3] A. Antoniou and A. F. Bastawros. Deformation characteristics of tin-based solder joints. *Journal of Materials Research*, 18:2304–2309, 2003.

[4] K. Autumn. Properties, principles, and parameters of the gecko adhesive system. In A. M. Smith and J. A. Callow, editors, *Biological Adhesives*, pages 225–255. Springer Verlag, Berlin, 2006.

[5] K. Autumn. Gecko adhesion: structure, function, and applications. *MRS Bulletin*, 32:473–478, 2007.

[6] K. Autumn, A. Dittmore, D. Santos, M. Spenko, and M. Cutkosky. Frictional

adhesion: a new angle on gecko attachment. *Journal of Experimental Biolog*, 209:3569–3579, 2006.

[7] K. Autumn and N. Gravish. Gecko adhesion: evolutionary nanotechnology. *Philosophical Transactions of the Royal Society A*, 366:1575–1590, 2008.

[8] K. Autumn and W. Hansen. Ultrahydrophobicity indicates a non-adhesive default state in gecko setae. *Journal of Comparative Physiology A*, 192:1205–1212, 2006.

[9] K. Autumn, S. T. Hsieh, D. M. Dudek, J. Chen, C. Chitaphan, and R. J. Full. Dynamics of geckos running vertically. *Journal of Experimental Biology*, 209:260–272, 2006.

[10] K. Autumn, Y. A. Liang, S. T. Hsieh, W. Zesch, W. P. Chan, T. W. Kenny, R. Fearing, and R. J. Full. Adhesive force of a single gecko foot-hair. *Nature*, 405:681–685, 2000.

[11] K. Autumn, C. Majidi, R. E. Groff, A. Dittmore, and R. Fearing. Effective elastic modulus of isolated gecko setal arrays. *Journal of Experimental Biology*, 209:3558–3568, 2006.

[12] K. Autumn, M. Sitti, Y. A. Liang, A. M. Peattie, W. R. Hansen, S. Sponberg, T. W. Kenny, R. Fearing, J. N. Israelachvili, and R. J. Full. Evidence for van der

waals adhesion in gecko setae. *Proceedins of the National Academy of Sciences of the United States of America*, 99:12252–12256, 2002.

[13] W. Barthlott and C. Neinhuis. Purity of the sacred lotus, or escape from contamination in biological surfaces. *Planta*, 202:1–8, 1997.

[14] S. Begej. Planar and finger-shaped optical tactile sensors for robotic applications. *IEEE Journal of Robotics and Automation*, 4:472–484, 1988.

[15] B. Bhushan and R. A. Sayer. Surface characterization and friction of a bio-inspired reversible adhesive tape. *Microsystem Technologies*, 13:71–78, 2007.

[16] C. Creton and P. Fabre. Vol. i - the mechanics of adhesion. In A. V. Pocius, D. A. Dillard, and M. Chaudhury, editors, *Adhesion science and engineering*, pages 535–576. Elsevier, Amsterdam, Netherland, 2002.

[17] A. J. Crosby, M. Hageman, and A. Duncan. Controlling polymer adhesion with "pancakes". *Langmuir*, 21:11738–11743, 2005.

[18] C. A. Dahlquist. In R. L. Patrick, editor, *Treatise on Adhesion and Adhesives*. Dekker, New York, 1969.

[19] W.-D. Dellit. Zur anatomie und physiologie der geckozehe. *Jena. Z. Naturw*, 68:613–656, 1934.

[20] L. Ge, S. Sethi, L. Ci, P. M. Ajayan, and A. Dhinojwala. Carbon nanotube-

based synthetic gecko tapes. *Proceedins of the National Academy of Sciences of the United States of America*, 104:10792–10795, 2007.

[21] A. K. Geim, S. V. Dubonos, I. V. Grigorieva, K. S. Novoselov, A. A. Zhukov, and S. Yu. Shapoval. Microfabricated adhesive mimicking gecko foot-hair. *Nature Materials*, 2:461–463, 2003.

[22] S. Gorb, M. Varenberg, A. Peressadko, and J. Tuma. Biomimetic mushroom-shaped fibrillar adhesive microstructure. *Journal of the Royal Society Interface*, 4:271–275, 2006.

[23] D. H. Gracias and G. A. Somorjai. Continuum force microscopy study of the elastic modulus, hardness and friction of polyethylene and polypropylene surfaces. *Macromolecules*, 31:1269–1276, 1998.

[24] N. Gravish, M. Wilkinson, and K. Autumn. Frictional and elastic energy in gecko adhesive attachment. *Journal of the Royal Society Interface*, 5:339–348, 2008.

[25] W. R. Hansen and K. Autumn. Evidence for self-cleaning in gecko setae. *Proceedins of the National Academy of Sciences of the United States of America*, 102:385–389, 2005.

[26] G. Huber, H. Mantz, R. Spolenak, K. Mecke, K. Jacobs, S. N. Gorb, and E. Arzt. Evidence for capillarity contributions to gecko adhesion from single

spatula nanomechanical measurements. *Proceedins of the National Academy of Sciences of the United States of America*, 102:16293–16296, 2005.

[27] C.-Y. Hui, L. Shen, A. Jagota, and K. Autumn. Mechanics of anti-fouling or self-cleaning in gecko. In *Proceedings of the 29th annual meeting of The Adhesion Society*, pages 29–31, Jacksonville, FL, 2006.

[28] J. N. Israelachvili. *Intermolecular & surface forces*. Academic Press, Oxford, 1991.

[29] K. L. Johnson. Adhesion and friction between a smooth elastic spherical asperity and a plane surface. *Proceedings: Mathematical, Physical and Engineering Sciences*, 453:163–179, 1997.

[30] K. L. Johnson, K. Kendall, and A. D. Roberts. Surface energy and the contact of elastic solids. *Proceedings of the Royal Society of London. Series A, Mathematical and Physical Sciences*, 324:301–313, 1971.

[31] K. Kendall. Thin-film peeling-the elastic term. *Journal of Physics D: Applied Physics*, 8:1449–145, 1975.

[32] S. Kim and M. Sitti. Biologically inspired polymer microfibers with spatulate tips as repeatable fibrillar adhesives. *Applied Physics Letters*, 89:261911, 2006.

[33] S. Kim, M. Spenko, S. Trujillo, B. Heyneman, V. Matolli, and M. Cutkosky. Whole body adhesion: hierarchical, directional and distributed control of ad-

hesive forces for a climbing robot. In *Proc. IEEE International conference on Robotics and Automation (ICRA'2007)*, pages 1268–1273, Roma, Italy, 2007.

[34] S. Kim, M. Spenko, S. Trujillo, B. Heyneman, D. Santos, and M. R. Cutkosky. Smooth vertical surface climbing with directional adhesion. *IEEE Transactions On Robotics*, 24:65–74, 2008.

[35] T. S. Kustandi, V. D. Samper, D. K. Yi, W. S. Ng, P. Neuzil, and W. Sun. Self-assembled nanoparticles based fabrication of gecko foot-hair-inspired polymer nanofibers. *Advanced Functional Materials*, 17:2211–2218, 2007.

[36] J. Lee and R. S. Fearing. Contact self-cleaning of synthetic gecko adhesive from polymer microfibers. *Langmuir*, 2008.

[37] J. Lee, C. Majidi, B. Schubert, and R. S. Fearing. Sliding-induced adhesion of stiff polymer microfibre arrays. i. macroscale behaviour. *Journal of The Royal Society Interface*, 5:835–844, 2008.

[38] C. Majidi. Remarks on formulating an adhesion problem using eulers elastica (draft). *Mechanics Research Communications*, 34:85–90, 2007.

[39] C. Majidi, R. E. Groff, Y. Maeno, B. Schubert, S. Baek, B. Bush, R. Maboudian, N. Gravish, M. Wilkinson, K. Autumn, and R. S. Fearing. High friction from a stiff polymer using micro-fiber arrays. *Physical Review Letters*, 97:076103, 2006.

[40] C. S. Majidi, R. E. Groff, and R. S. Fearing. Attachment of fiber array adhesive through side contact. *Journal of Applied Physics*, 98:103521, 2005.

[41] M. P. Murphy, B. Aksak, and M. Sitti. Adhesion and anisotropic friction enhancements of angled heterogeneous micro-fiber arrays with spherical and spatula tips. *Journal of Adhesion Science and Technology*, 21:1281–1296, 2007.

[42] N. J. Glassmaker NJ, A Jagota, C.-Y. Hui, W. L. Noderer, and M. K. Chaudhury. Biologically inspired crack trapping for enhanced adhesion. *Proceedins of the National Academy of Sciences of the United States of America*, 104:10786–10791, 2007.

[43] M. T. Northen and K. L. Turner. Meso-scale adhesion testing of integrated micro- and nano-scale structures. *Sensors and Actuators A: Physical*, 130-131:583–587, 2006.

[44] I. Novák. Effect of surface pretreatment on wettability of polypropylene. *Journal of Materials Science Letters*, 15:1137–1138, 1996.

[45] A. M. Peattie, C. Majidi, A. Corder, and R. J. Full. Ancestrally high elastic modulus of gecko setal β-keratin. *Journal of The Royal Society Interface*, 4:1071–1076, 2007.

[46] B. N. J. Persson. Biological adhesion for locomotion: basic principles. *Journal of Adhesion Science and Technology*, 21:1145–1173, 2007.

[47] B. N. J. Persson and S. Gorb. The effect of surface roughness on the adhesion of elastic plates with application to biological systems. *The Journal of Chemical Physics*, 119:11437–11444, 2003.

[48] A. V. Pocius. *Adhesion and adhesive technology.* Hanser, Munich, 2002.

[49] C. M. Pooley and D. Tabor. Friction and molecular structure: the behaviour of some thermoplastics. *Proceedings of the Royal Society of London. Series A, Mathematical and Physical Sciences*, 329:251–274, 1972.

[50] L. Qu and L. Dai. Gecko-foot-mimetic aligned single-walled carbon nanotube dry adhesives with unique electrical and thermal properties. *Advanced Materials*, 19:3844–3849, 2007.

[51] R. Ruibal and V. Ernst. The structure of the digital setae of lizards. *Journal of Morphology*, 117:271–293, 1965.

[52] D. Santos, S. Kim, M. Spenko, A. Parness, and M. Cutkosky. Directional adhesive structures for controlled climbing on smooth vertical surfaces. In *Proc. IEEE International conference on Robotics and Automation (ICRA'2007)*, pages 1262–1267, Roma, Italy, 2007.

[53] D. Santos, M. Spenko, A. Parness, S. Kim, and M. Cutkosky. Directional adhesion for climbing: theoretical and practical considerations. *Journal of Adhesion Science and Technology*, 21:1317–1341, 2007.

[54] H. Schmidt. Zur anatomie und physiologie der geckopfote. *Jena Z. Naturw*, 39:551–580, 1905.

[55] B. Schubert, J. Lee, C. Majidi, and R. S. Fearing. Sliding-induced adhesion of stiff polymer microfibre arrays. ii. microscale behaviour. *Journal of The Royal Society Interface*, 5:845–853, 2008.

[56] B. Schubert, C. Majidi, R. E. Groff, S. Baek, B. Bush, R. Maboudian, and R. S. Fearing. Towards friction and adhesion from high modulus microfiber arrays. *Journal of Adhesion Science and Technology*, 21:1297–1315, 2007.

[57] S. Sethi, L. Ge, L. Ci abd P. M. Ajayan, and A. Dhinojwala. Gecko-inspired carbon nanotube-based self-cleaing adhesives. *Nano Letters*, 8:822–825, 2008.

[58] M. Sitti. Atomic force microscope probe based controlled pushing for nanotribological characterization. *IEEE/ASME Transactions on Mechatronics*, 9:343–349, 2004.

[59] M. Sitti and R. S. Fearing. Synthetic gecko foot-hair micro/nano-structures as dry adhesives. *Journal of Adhesion Science and Technology*, 17:1055–1073, 2003.

[60] M. Varenberg and S. Gorb. Shearing of fibrillar adhesive microstructure: friction and shear-related changes in pull-off force. *Journal of The Royal Society Interface*, 4:721–725, 2007.

[61] H. Yao, G. Della Rocca, P.R. Guduru, and H. Gao. Adhesion and sliding response

of a biologically inspired fibrillar surface: experimental observations. *Journal of The Royal Society Interface*, 5:723–733, 2008.

[62] M.-F. Yu, T. Kowalewski, and R. S. Ruoff. Structural analysis of collapsed, and twisted and collapsed, multiwalled carbon nanotubes by atomic force microscopy. *Physical Review Letters*, 86:87–90, 2001.

[63] Y. Zhao, T. Tong, L. Delzeit, A. Kashani, M. Meyyappan, and A. Majumdar. Interfacial energy and strength of multiwalled-carbon-nanotube-based dry adhesive. *Journal of Vacuum Science and Technology B*, 24:331–335, 2006.